Universiteit Utrecht

Opleiding Natuur- en Sterrenkunde

Pelagic tidal measurements from deep sea pressure sensors across the Mozambique Channel and eastern Madagascar

Bachelor Thesis

Pim Breedijk

Supervisors:

prof. dr. L.R.M. Maas
IMAU

Borja Aguiar-Gonzalez
University of Delaware, USA

Leandro Ponsoni
Université catholique de Louvain, Belgium

June 14, 2017

Abstract

One year records of sea bottom pressure have been used on multiple sites in the Mozambique Channel and near the coast of Eastern Madagascar. This data has been used to collect the amplitude and Greenwich phase of as many tidal constituents as possible. This has been done using a method called harmonic analysis and been performed by the T_TIDE program. The collected amplitudes and phase angles have then been compared to altimeter data for the same region. This comparison delivered relatively large differences. This leads us to believe that the results from the deep sea measurements must first be improved and inaccuracies in the altimeter data should be considered before further conlusions can be drawn.

Contents

1 Introduction

This research focuses on collecting the phase and amplitude of tidal constituents in the Mozambique Channel and on the eastern coast of Madagascar. The collected data on the two sites will be compared with one another and will also be compared to altimeter data in the same area. This may be used to improve tidal models and to learn more about the internal tides in this specific area. This paper describes how to analyze the collected data using a program called T_TIDE, which uses harmonic analysis to gather the information we want.

1.1 History of tides

For those who live by the sea, tides are a familiar phenomenon. The relationship between high water and lunar phases are embodied in for example medieval tide tables. Practical need for this relationship has always been present. In the earlier days for harbor management, protection from flooding and coastal navigation. In more recent times it is more concerned with amphibious military operations, harnessing tidal power[1] and precise corrections to measurements to and from artificial satellites.

Early theories on tides were formed by people like Descartes and Galileo. These theories were later proved inadequate by Isaac Newton. Newton's laws on gravitation shed a new light on tidal generating forces and explained how the Moon and the Sun influence the tides. Further pioneering work on the dynamics of tides was done by Pierre-Simon Laplace. Laplace formulated a set of linear differential equations, known as Laplace's tidal equations, which describe the tidal flow. Because of the complicated nature of these equations, and no tools to measure the behavior of tides in mid-oceans, tides have moved to the background of scientific research. One of the big breakthroughs in tidal prediction was the idea of harmonic analysis, introduced by William Thomson, the later Lord Kelvin. This method of analysis provided accurate predictions at any site where tides had been measured for a long enough period of time.

In modern days, research of tides is mainly focused around measuring the tides and comparing the data to satellite altimetry to improve tidal models and to learn more about internal tides[2]. The long period of tides requires long term measurements to get meaningful results. This means it is a very time- and money consuming process to gather data all around the world. Therefore, local measurements of tides are limited. As we can see in Fig. 1, there have been done deep-ocean measurements of tides all around the world, but very few in the Indian Ocean and around Madagascar. Satellite altimetry gives a solution for this problem, because satellites circling the Earth can measure sea surface elevations, and therefore tides. The upside is that in this way, tides can be measured all around the world in relatively quick

[1] For an example of this, see http://www.bluewater.com/new-energy/texel-project/

[2] The ocean consists of different layers with different density. The boundary between these layers fluctuates up and down. These fluctations are what is called internal tides. Internal tides are generated mainly by surface tides and wind.

fashion. The downside, however, to these kind of measurements is the resolution. Local deep-ocean measurements can acquire much greater resolution and therefore a more correct view of the local tides. Comparing these two methods of measuring tides and correcting both to each other, gives good empirical data to construct global tidal models.[1]

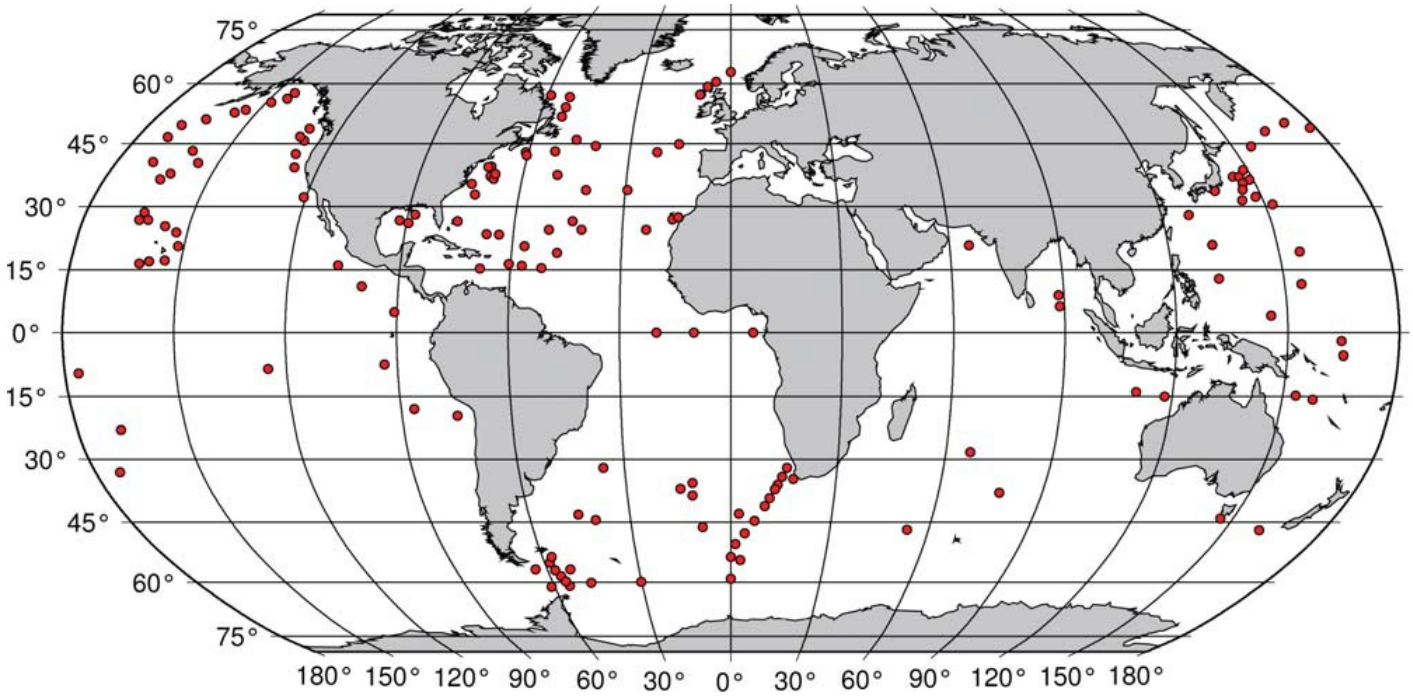

Figure 1: Locations of the 151 deep-ocean bottom-pressure stations.[2]

2 Theory

2.1 Theory of tides

The rise and fall of water along coasts, known as the tides, is one of the most reliable phenomena known to mankind. But what exactly are these tides? Tides are waves that move through most of the seas and oceans. These waves, with very long periods and wavelengths are a response to forces exerted by the Sun and the Moon.
Since Newton's Principia, published in 1687, we know that two bodies gravitate towards each other. Gravitation acting on the deformable fluid mantle called ocean is what causes tides. The force exerted by the Moon and the Sun on the ocean results in tidal waves. This tide generating force can be expressed as follows:

$$F_{tid} \propto \frac{M}{r^3}. \tag{1}$$

Where M is the mass of the body acting on the oceans, and r is the distance from this body to the Earth. From this relation follows that the tide-generating force by the Sun is about half that of the Moon, see Fig. 2. Therefore, the Moon is the dominant factor affecting

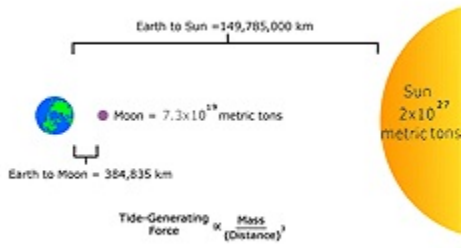

Figure 2: The Earth−Moon−Sun system.[3]

tides on the Earth.

Since most places on Earth experience high tide and low tide approximatly two times per day, we know that gravity is not the only force causing tides. The other force known to cause tides is inertia. Inertia is the resistance of any moving object to change its motion, or its tendency to move in a straight line. This tendency counterbalances gravity. Inertia and gravity together cause the two major tidal bulges on Earth as seen in Fig. 3.

Since we know inertia is a reaction to the forces exerted by the Sun and the Moon, we can now look at what causes variations in the tidal height. One cause for variation is the allignment of the Sun, Moon and Earth. When these three are in a straight line to each other, the forces cause extra high high-tides and extra low low-tides, this is called spring tide. When the Sun and the Moon are at a right angle, as seen from the Earth, the two tidal forces partially cancel each other out. This causes high tide and low tide to have less difference, or be more moderate. This is what we call neap tide. Also of interest to this are the distances between the Earth and the Sun and the Moon. Since the Moon follows an elliptical inclined path around the Earth, and the Earth follows an elliptical path around the Sun, the tides will vary overtime due to this.[**?**]

Apart from gravitation by the Sun and the Moon, there is one more big factor in the compexity of tides. This factor is the irregular configuration of the ocean bottom and lateral boundaries[4], or bathymetry. Since the effect of bathymetry on tides is so complex, it is nearly impossible to model the tides correctly. Therefore, to still gain knowledge of global

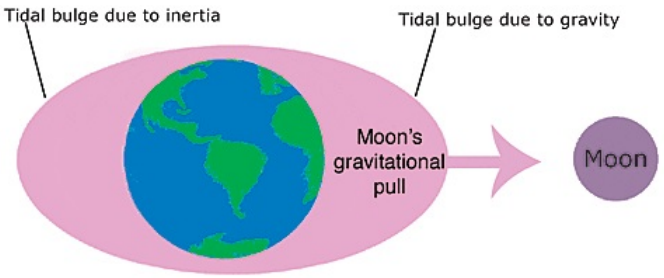

Figure 3: Sketch of the tidal bulges.[3]

tides, measurements of tides are necessary.

2.2 Tidal resonance

Just like any other mechanical system in oscillation, the ocean is bound to resonance. Resonance is the tendency of a system to absorb more energy, or show greater amplitude at a certain frequency. This frequency is called the natural frequency. In the ocean this typically leads to big differences in high and low tide. Famous examples of this are found in the Bay of Fundy and in the Bristol Channel.
An important assumption leading from the oceanic response to resonance is the "credo of smoothness", imposed by Cartwright and Munk in 1966 [5]. This credo of smoothness states that there are no sharp resonance peaks. This means that the admittance is not allowed to vary dramatically as a function of frequency for any one frequency band. So, for close frequencies, the ocean should not behave very different in response to close frequencies. Due to this assumption, we expect the phase angles in the different frequency bands to vary smoothly. The relation for the amplitudes in the different frequency bands is more complex and will not be discussed in this research.

2.3 Data collection

2.3.1 Deep sea measurements

The data used in this research are deep sea pressure measurements. This data is collected by moorings deployed at the locations shown in Fig.4 for the Mozambique Channel and in Fig.5 for the ones located near Eastern Madagascar. A mooring is a collection of devices attached to a wire. This wire is anchored to the ocean floor and the top is often held afloat with a buoy. Instruments often found on moorings are CTDs[3], current meters and biological sensors. In the Mozambique Channel, these pressure measurements are performed by MicroCATs[4], while in the EMC[5] these are done by ADCPs[6].
Before we perform harmonic analysis (see section 2.4.2) we want to convert the pressure measurements to depth measurements. This is not necessary since the most important property here is the tidal signature in the time series. Converting to depth measurements does however make it easier to "read" the outcome of the harmonic analysis. A way to do this is explained by Ray[2]. A summary of this will be given here.

The conversion of bottom pressure to sea surface heigths in an inhomogeneous ocean in which internal tides occur is quite a complex subject. Since global maps of internal tides are too unreliable, the effects of these internal tides can not be taken into account in any systematic way. However, because this is still ongoing research, in a future time this influence should be reconsidered since it could result in improved precision between bottom pressure and altimetric tides. Now follows the way to convert bottom pressure to sea surface elevation.

[3]Device used to measure conductivity, temperature and pressure.
[4]Used to measure conductivity, temperature and pressure.
[5]EMC = Eastern Madagascar Current.
[6]Acoustic Doppler Current Profiler, used to measure water current velocities using the Doppler effect. Can also measure sea surface height.

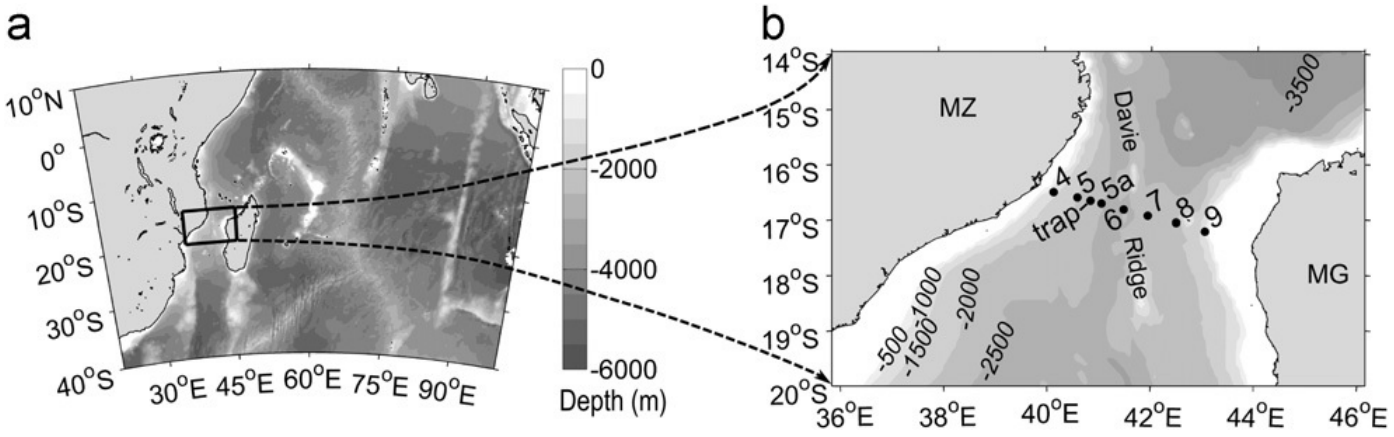

Figure 4: Overview map of the southwest Indian Ocean (a) with the location of the mooring section at the narrowest part of the Mozambique Channel enlarged (b). Shading indicates depth (m)[6].

Consider a point in the ocean at depth H. The bottom pressure is given by $gH\rho_{mean}$, where g is the gravitational acceleration and ρ_{mean} is the mean density of the water column. Now consider a tidal convergence at this location, which increases mass at every level of the water column by a fraction ϵ. The fluctuation of the sea surface height, η, is ϵH if compression of the water column is ignored. With this compression accounted for, it would be slightly less. Following this increase of sea surface height, the pressure then also increases by the same fraction ϵ. This means the local density increases by $\partial\rho/\partial p = 1/c^2$, where c is the speed of sound.
Thickness of the water column can change in two ways. First, increasing by ϵ from the additive mass. Second, decreasing by compression from the extra overlaying mass. This mean the thickness changes by $\epsilon(1 - p/\rho c^2)$. The second correction term is roughly gz/c^2 at depth z, so the average of this over the water colum is $gH/2c^2$. So, for a bottom pressure tidal fluctuation δp_b the surface elevation is given by

$$\eta = \delta p_b \frac{1 - gH/2c^2}{g\rho_{mean}}. \tag{2}$$

Looking at the $\frac{gH}{2c^2}$ term in this equation, if we fill in a typical depth of 2000 meter, we find that this term is about $\frac{gH}{2c^2} \simeq \frac{1}{9*10^{12}}$. Since $1 >> \frac{1}{9*10^{12}}$ we can estimate eq. 2 to be

$$\eta = \frac{\delta p_b}{g\rho_{mean}}. \tag{3}$$

2.3.2 Altimeter data

The altimeter data used is data provided by Zaron [8]. This data contains amplitude and phase data for ten tidal constituents worldwide. The data set is called GOT−e, which means that this uses the GOT[7] empirical model and extrapolates it so shorelines are also included. The amplitude and phase angle data collected by these altimeter satellites for the location relevant to this research can be found in appendix B.

[7]Goddard/Grenoble Ocean Tide

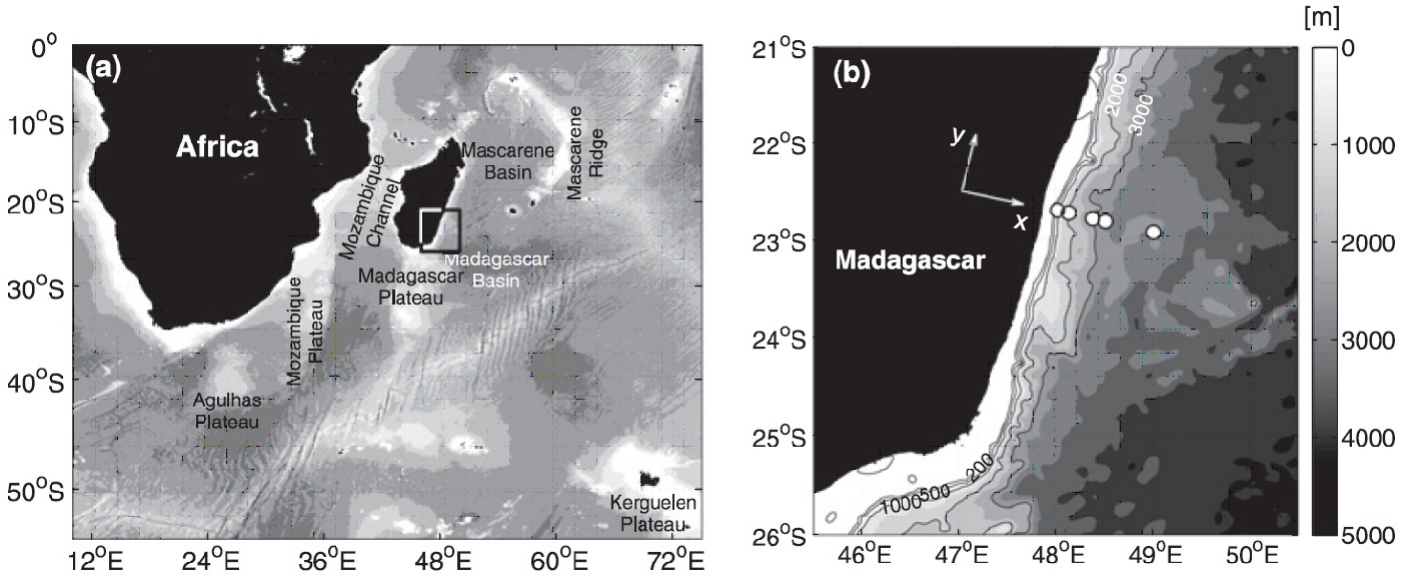

Figure 5: (a) Map of the southwest Indian Ocean. (b)Zoom of the area of study demarcated by the square drawn in (a). Bathymetric contours are drawn in shades of gray. The white circles represent the geographical location of the moorings (EMC1-EMC5, from inshore to offshore)[7].

2.3.3 Instrument depth

While collecting tidal data, it is preffered to use measurements from the bottom of the ocean. In this way there is the least amount of noise from internal tides and instruments slipping from the line for example. When looking at instruments who are not recording on the bottom of the ocean, these factors should be taken into consideration, or at least should be discussed when analysing the data. The depth of the instruments used and the total water depth at these locations are shown in table 1. We see here that the EMC instruments return true bottom pressure measurements, while in the Mozambique Channel There are no devices on the bottom of the ocean. There are however some devices really close to the bottom, these are lmc5, lmc5a -3623 and lmc8. The data from these devices can be considered bottom pressure measurements while for the rest of the data other factors should also be considered in the analysis.

2.4 Fourier and Harmonic analysis

Extracting information from big datasets is one of the most important tasks of research of tides. Since we know tides are waves we can apply two methods often used in data analysis. These methods are called Fourier analysis and Harmonic analysis.

Table 1: Table showing the depth at which the different instruments record and also the total water depth at that location.

	Depth device (m)	Total depth (m)
lmc4	1100	1351
lmc5	1966	1992
lmc5a −2655	1975	2402
lmc5a −3623	2375	2402
lmc6	2350	2691
lmc7	1520	1995
lmc8	2125	2199
lmctrap	1950	2241
EMC1	500	500
EMC3	2600	2600

2.4.1 Fourier analysis

According to Fourier's theorem, any function $f(t)$, can be described by a series of sines and cosines of increasing frequencies. This series is called the spectral distribution

$$\hat{f}(k) = \int_{-\infty}^{\infty} f(t) e^{-2\pi i k t} dt. \tag{4}$$

This definition, however, is for functions existing on an infinite interval, while physically observed functions are obtained over a finite time interval. This alters the Fourier transformation and the spectral distribution from a continuous spectrum $\hat{f}(k)$, to a discrete spectrum f_n. In the case of deep-ocean measurements to the pressure, we have a finite number of observations obtained at discrete time increments. This means there are as much Fourier coefficients as there are observations. Hence, the discrete spectrum forms a one-to-one representation of the data.

Performing a Fourier analysis on observed data gives a frequency spectrum which shows what frequencies are most dominant in the measured signal. This spectrum is often displayed as a power spectral density, from now on referred to as PSD. The PSD is an energy spectrum and shows how the energy in a wave signal is distributed over the different frequencies.

Another thing to consider while analyzing a non−infinite time series, is that the data does not come in smoothly, but starts instantly. One way to work around this is to use a so called tapering− or window function. This function is zero outside of a chosen interval. In the case of this research, we want the tapering function to make sure the data starts off smoothly so we get a cleaner Fourier analysis. For constructing the PSD, we use a so called Hanning window. In MATLAB, the Hanning window is computed as follows[9]

$$w(n) = \frac{1 - \cos(2\pi \frac{n}{N})}{2}, 0 \leq n \leq N. \tag{5}$$

The window length $L = N + 1$ must be specified here and in this case will be $L = 389F_s$, where F_s is the number of measurements per hour.

2.4.2 Harmonic analysis

To get a better description of an observed signal, it is usefull to look at the cause of variability. In case of the tides, there is precise knowledge of the dynamics of the Sun, Moon and Earth. It can be argued that there are a few precisely described frequencies at which tidal forcing occurs. While these frequencies could be incorporated in the equations of motion, local bathymetry makes it impossible to make reliable tidal models. Acknowledging this inablity leaves us with the knowledge of these frequencies which can be used in harmonic analysis. For harmonic analysis, in contrast to Fourier analysis, the frequencies do not need to be multiples of each other and, because the frequencies of the forcing are known, a fixed sampling period is not required. Therefore harmonic analysis can deal with data gaps.

Just as Fourier analysis, harmonic analysis is a mathematical tool to obtain knowledge of observed time series. Harmonic analysis does so by creating a model. This model consists of, at first, sines and cosines at the prescribed frequencies. Later, thanks to nonlinearities in the hydrodynamic equations, also sums and differences of these fundamental frequencies may appear.

This next example showing how harmonic analysis is performed[10].
Consider observing sea surface elevation ζ at times t_m, denoted as ζ_m. We are looking for a model $\hat{\zeta}$ with a single frequency ω,

$$\hat{\zeta} = C\cos\omega t + S\sin\omega t. \tag{6}$$

Here C and S are the amplitudes we want to determine. First of, one needs to remove the time average of the measurements. Suppose now, we sample the signal, so $\hat{\zeta}_m = \hat{\zeta}(t_m)$, at times t_m, $m \in \{1, M\}$. Now, C and S are obtained by minimizing

$$D = \sum_{m=1}^{M} (\zeta_m - \hat{\zeta}(t_m))^2. \tag{7}$$

This minimum is obtained when both partial derivates $D_C = 0$[8] and $D_S = 0$. Taking these partial derivatives gives

$$\sum_{m=1}^{M} (\zeta_m - \hat{\zeta}(t_m))\cos\omega t_m = 0, \tag{8}$$

and

$$\sum_{m=1}^{M} (\zeta_m - \hat{\zeta}(t_m))\sin\omega t_m = 0. \tag{9}$$

Solving this system yields the amplitudes C and S as a result. This method can be extended to multi-frequency models, containing N independent frequencies, ω_n, $n \leq N$, with amplitudes C_n and S_n.

[8]Here we use the subscript derivative convention, where $D_C = \frac{\partial D}{\partial C}$.

2.5 T_TIDE

For this research, the harmonic analysis will be performed using T_TIDE. This program, developed using MATLAB, specialises in performing a harmonic analysis for tidal analysis. For a detailed explanation of how T_TIDE works, see[11]. In short, it comes down to this. T_TIDE performs classic harmonic analysis with some user specified options like nodal corrections and inference. Inference is a method where constituents with close frequencies are solved for time series with insufficient resolution or record length. Since we are dealing with time series of one year with a good resolution, inference will not be used. Nodal corrections will be discussed in chapter 2.6.

T_TIDE models the tidal component of the data as follows:

$$\zeta(t) = \sum_n A_n \cos(\frac{2\pi}{T_n}t + \phi_n). \tag{10}$$

Where, $\zeta(t)$ is the sea surface elevation as a function of time t, A_n is the amplitude of constituent n, T_n is the period of this constituent and ϕ_n is the Greenwich phase of this constituent. The Greenwich phase is defined as the phase referenced to the phase of equilibrium response at 0^o longitude. T_TIDE then aims to find A_n and ϕ_n using the method of least squares like explained in the section on harmonic analysis.

2.6 Nodal corrections

As mentioned, T_TIDE gives the user an option to perform nodal corrections. In tidal analysis, to resolve the very narrow nodal band, a measuring period of at least 19 years[9] is required. When records of this long are not available it is customary to use periods of one year to analyse as the standard length. This one year period normally suffices to get a correct measurement for the main diurnal and semidiurnal constituents. When this is done, there must be noticed that there still is influence from the constituents with periods longer than one year. These frequencies will not be taken account for in the model, but still are there in the "real world" and therefore will effect the measurements and the results we obtain for the other constituents. Here follows a short description of how nodal corrections are performed, closely following[4]. For the exact way this is done in T_TIDE, see the paper by Pawlowicz[11].

Let C be the amplitude of a constituent and let $E \equiv \omega t + s\lambda + \phi$ be the argument of this constituent. Similarly, for the nodal terms we write C_k and $E_k = (\sigma + k|\Delta\sigma|)t + s\lambda + \phi_k$, where $|\Delta\sigma|$ represents the spacing of lines in the nodal band and $k = \pm 1, \pm 2, \pm 3, ...$ is the order of a particular line. Then formally

$$\zeta(t) = fC\cos(E + u) = C\cos(E) + \sum_k C_k \cos E_k, \tag{11}$$

where $f(t)$ and $u(t)$ are the amplitude and phase of the modulation,

[9] Note that it is not currently possible with T_TIDE.

$$fe^{iu} \equiv 1 + C^{-1} \sum_k C_k e^{i(k|\Delta\sigma|t+\phi_k-\phi)}, \tag{12}$$

that result from superposition. Here, the first-order terms, $k = \pm 1$ are always dominant. These first-order terms have a period of $360^o/|\Delta\sigma|$, which equal to 18.6 years for the nodal bands. Due to this, we may regard f and u to be constant over intervals of a year or less. Therefore, nodal terms are usually taken into account by writing the series as

$$\sum_j f_j C_j \cos(\sigma_j t + s\lambda + \phi_j + u_j). \tag{13}$$

In this way, nodal terms are excluded from the sum. Their effect, however, is implicit in the node factor f_j and the phase modulation u_j. The effect of nodal corrections is shown in Fig. 6.

3 Results

In this chapter, the gathered data will be analysed and the results gained using T_TIDE will be presented and shortly discussed. The results will be presented as follows. For each location, shown in Fig. 4 and Fig. 5, a one year analysis has been performed. The starting dates have been synchronized as close as possible. Each figure shows four plots. The top one shows the gathered data, the model acquired using harmonic analysis and the two subtracted from each other. The second plot shows the amplitude for all the significant constituents. Significant here means that the constituent has a signal-to-noise ratio (SNR) of SNR > 1. The SNR is calculated as the squared ratio of the amplitude and error in the amplitude[11]. The third plot shows the value of the Greenwich phase for the significant constituents. The fourth plot in each figure shows two lines. One line is the total energy. The other one shows the residual energy, this is the energy present after removing the tidal energy. There is also a dashed line present, which marks the inertial frequency. This is the frequency at which an energy bump should be present due to the rotation of the earth.
Besides the results from the harmonic analysis, there will also be tables showing the difference in amplitude and phase between the deep sea measurements and the altimeter data from the GOT−e 4.7 Ocean Tide file. The tables also contain an error. This is the error T_TIDE produces for each constituent. This means that if the error is bigger than the difference, there is agreement between the deep sea measurement and the altimeter data.

3.1 Time drift

With these kind of measurements it is standard to check the instruments, and in particular the internal clock, before and after the moorings are deployed. This is done because the internal clocks drift over time and this has influence on the measurements. The check when the instruments are recovered is to see how far the clock has drifted so this effect can be accounted for. For the instruments deployed in the Mozambique Channel this check during the recovery was not performed. Therefore, we assume there might be a time drift in these measurements. In this paper I will not account for the effect of this assumed time drift.

However, I will show a way to make it presumable that there indeed is a time drift present in the data.
First of, the phase angles produced by T_TIDE all relate to the same reference time. We suppose that a time drift may lead to a phase drift. So, to see if there is a time drift in the measurements, we look at the time evolution of the phase angles. For now we only want to see if there might be a time drift present, so we will look at the Greenwich phase for the M2 constituent recorded by lmc5 − 4346. This particular data set is chosen because it is one of the closest to the bottom. The following check was suggested by Leo Maas during personal communication.
We want to look at the time evolution of the M2 phase. To do this, we let T_TIDE analyse a period of 183 days. Then, we shift the beginning of this series by 47 days and perform the same analysis. We do this using the complete data set, which consists of 658 days of data, so we get 14 snapshots of the evolution of the M2 phase. Ideally, if there is no time drift, all these phase angles would be the same. In the presence of a time drift, the phase angles are not the same and are expected to steadily increase or decrease. It is important to notice that such an increase or decrease might be due to the influence of long period tides, like explained in chapter 2.6. This influence can however be accounted for in T_TIDE. After concluding if there is a time drift present, it is also interesting to repeat the same process, but now looking at the amplitude of the constituent, to see if this is also influenced by the time drift. In Fig. 6 we can see the slow time evolution of the phase and the amplitude of M2. We see one line where nodal corrections have been applied and one line without nodal corrections. It is clear to see that both the phase and the amplitude increase slowly over time. Assuming this increase comes solely from time drift we find an increase of 0.0038 degrees per day for the phase angle and an increase of $6.84 \cdot 10^{-5}$ meter per day for the amplitude.
Physically, a phase shift can be seen as a time shift. If a wave with period T is phase shifted by $\Delta\phi$, this relates to a time shift

$$\Delta\phi = \frac{2\pi}{T}\Delta t. \tag{14}$$

Since we are looking at the M2 constituent with a period of $T = 12.42$ hr, we have measured a time drift of 0.18 seconds per day or about 66 seconds in a year.

3.2 Mozambique Channel

3.2.1 Mooring lmc4 − 4352

The results from the analysis for lmc4 − 4352 are shown in Fig. 7. In the top plot we see a lot of peaks in the sea surface elevations. We know that these are related to non-tidal events, since the red line (showing the data minus the tidal model) follows these peaks almost exactly. These peaks can have several causes. These causes normally are high energetic events in either the atmosphere or the ocean itself. Examples of these high energetic events that can cause this are tropical storms, hurricanes and eddies. In the second plot, we see that the strongest constituents (the ones with the highest amplitudes) are found in the diurnal (around 0.04 cph[10]) and semidiurnal (around 0.08 cph) band. The strongest constituents are M2 and S2. Significant amplitudes with the highest frequency appear in the band around

[10]cph = cycles per hour.

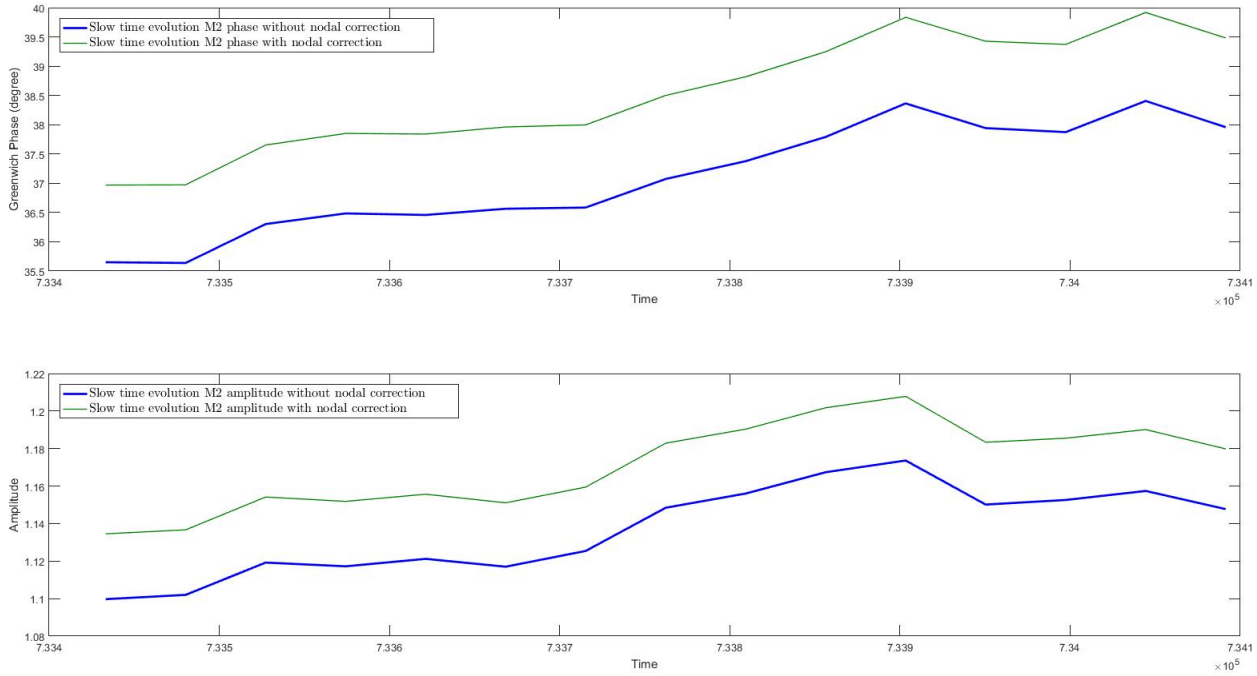

Figure 6: Slow time evolution of M2 amplitude and phase angle. Using intervals of 183 days. Time plotted here is in days.

0.16 cph. The third plot in the figure shows us the Greenwich phase of the constituents. One thing to notice immediately is that in the different bands, the phases are all "grouped up" with the exception of the MKS2 constituent. The fact that the rest of the phases are grouped up is a good sign and shows that the results follow the credo of smoothness. In the last plot, we see high peaks in the energy at the diurnal and semidiurnal bands. Notice that in the residual energy, there still are peaks at these tidal frequencies.

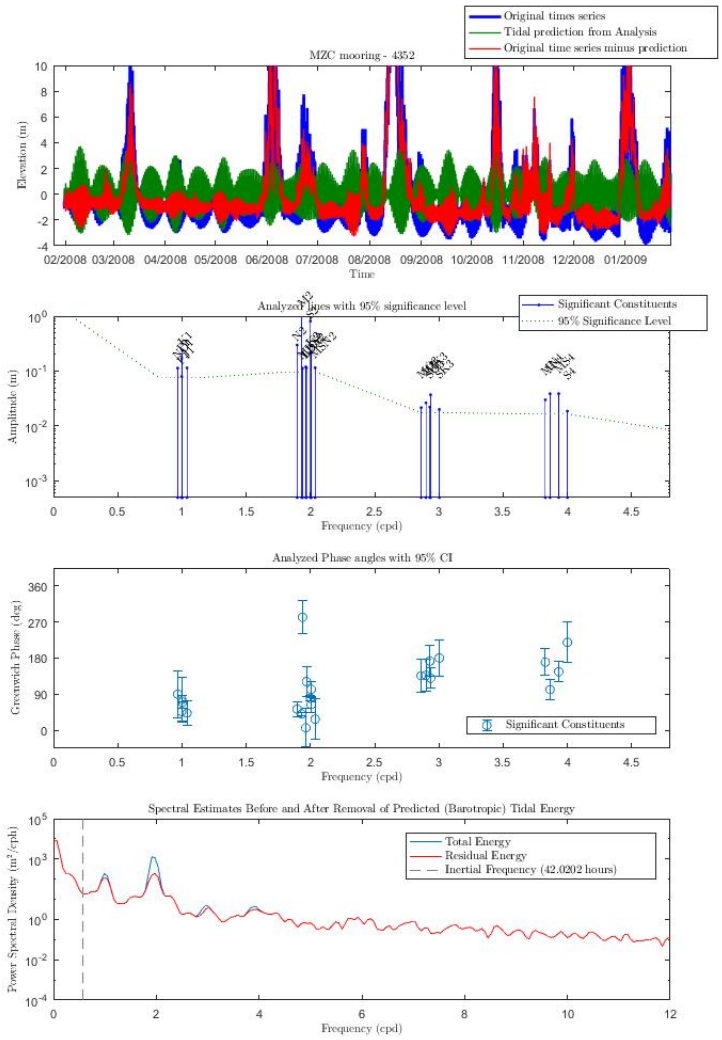

Figure 7: Results of T_TIDE analysis for lmc4.

Table 2: Difference in amplitude and phase between the deep sea measurements and altimeter data for the lmc4 location. Amplitude difference is in cm and phase difference is in degrees.

	K1	K2	M2	M4	N2	O1	P1	Q1	S2
Amplitude difference	18.0 ± 7.5	5.04 ± 9.7	27.98 ± 9.7	3.1 ± 1.6	11.0 ± 9.7	nvt	5.9 ± 7.5	nvt	20.5 ± 9.7
Phase difference	158.24 ± 16.28	11.47 ± 20.26	4.35 ± 4.12	99.75 ± 25.79	34.84 ± 19.04	nvt	174.46 ± 54.03	nvt	3.427 ± 6.82

3.2.2 Mooring lmc$5-4346$

Next are the results from the analysis on the data collected by lmc$5-4346$, show in Fig. 8. The top plot shows a few peaks to sea surface elevation which are not caused by the tides. Notice that there are less peaks than at the lmc4 location and the peaks are also a lot less high (Up to 12 m at lmc4 while only up to 7 meter at lmc5). The second plot shows that, in this location the main constituents are also in the diurnal and semidiurnal bands but the frequency of significant constituents reaches nearly 0.25 cph. Another notable difference is the presence of a long period constituent, SSA, short for Solar Semi-Annual. The SSA constituent here, has a bigger amplitude than important constituents like N2 and K2, showing that long period constituents can be a big factor in water elevation. Next, looking at the phase angles, we see that the phases are grouped up per band once again. Also again apart from the MKS2 constituent. It may look that in de diurnal band there are also two constituents (Q1 and BET1) who are not grouped up. But since these two are grouped around 360^o and the other ones around 0^o it still appears as though the credo of smoothness is followed. For the PSD we conclude the same as for the lmc4 location, there are strong peaks at the tidal frequencies which seem to be smaller for the residual energy, although still present there.

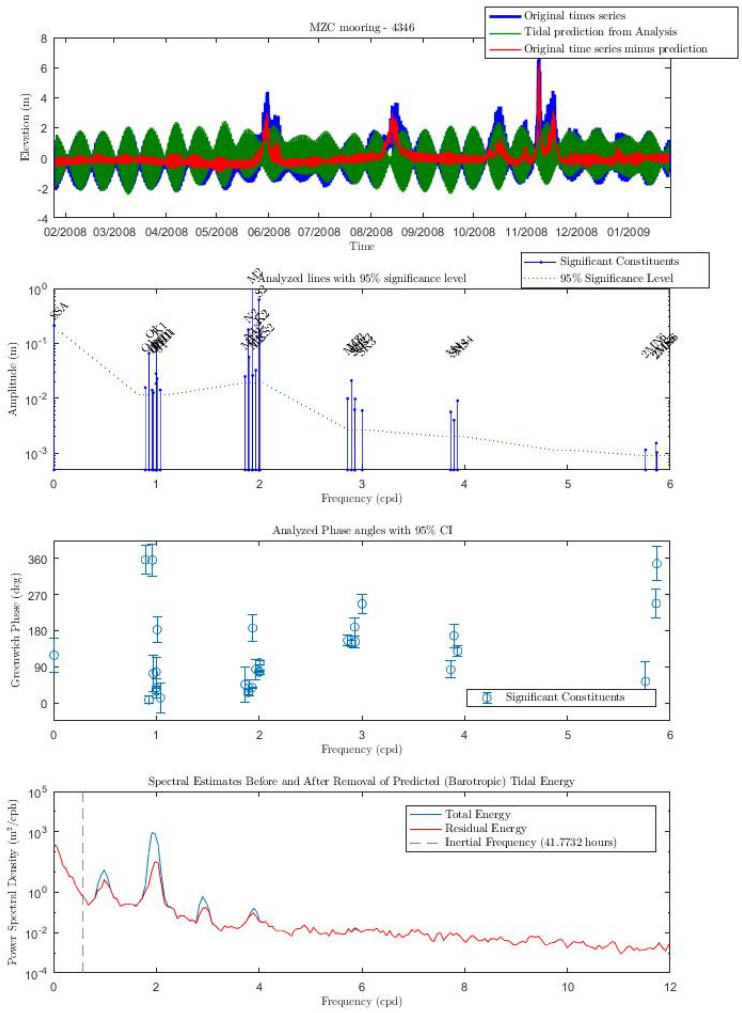

Figure 8: Results of T_TIDE analysis for lmc5.

Table 3: Difference in amplitude and phase between the deep sea measurements and altimeter data for the lmc5 location. Amplitude difference is in cm and phase difference is in degrees. The error is the same error as T_TIDE gives for amplitude and phase. This means that if the error is bigger than the difference, the deep sea measurements and altimeter data agree.

	K1	K2	M2	M4	N2	O1	P1	Q1	S2
Amplitude difference	2.0 ± 1.2	0.2 ± 1.9	4.32 ± 1.9	0.1 ± 0.2	1.3 ± 1.9	0.6 ± 1.2	0.6 ± 1.2	0.0061 ± 1.2	1.3 ± 1.9
Phase difference	26.74 ± 7.21	1.76 ± 5	2.12 ± 0.96	80.81 ± 21.49	8.85 ± 6.2	347.46 ± 8.73	34.48 ± 23.94	20.91 ± 34.99	1.56 ± 1.72

3.2.3 Mooring lmc5a −2655

For the lmc5a location, there are actually two measuring stations. First is the one with serial number 2655 and second is the one with serial number 3623. Station 2655 is located higher up the line and is therefore more influenced by internal tides and fluctuations of the line,

which give extra fluctuations in pressure.
Looking at the time series obtained by station 2655 we see a lot of events where the water level raises over 18 m. It is also noticeable that some of these events last for over two months. Looking at the amplitudes for the significant constituents we see once again high amplitudes in the diurnal and semidiurnal bands and frequencies reaching 0.25 cph. Also notice here that the amplitudes are noticeably higher than those at the lmc4 and lmc5 locations. Looking at the phase angles, we notice two constituents that fall out of line in the diurnal band, NO1 and J1. The N2 constituent looks to be out of line but, like with the ones at the lmc5 location, since this one is located around 360^o and the other constituents in the semidiurnal band around 0^o they still are regarded as grouped up and therefore we conclude that the credo of smoothness is followed. In the energy spectrum, the only noticeable difference with the other locations is that we see a small peak here located at the inertial frequency.

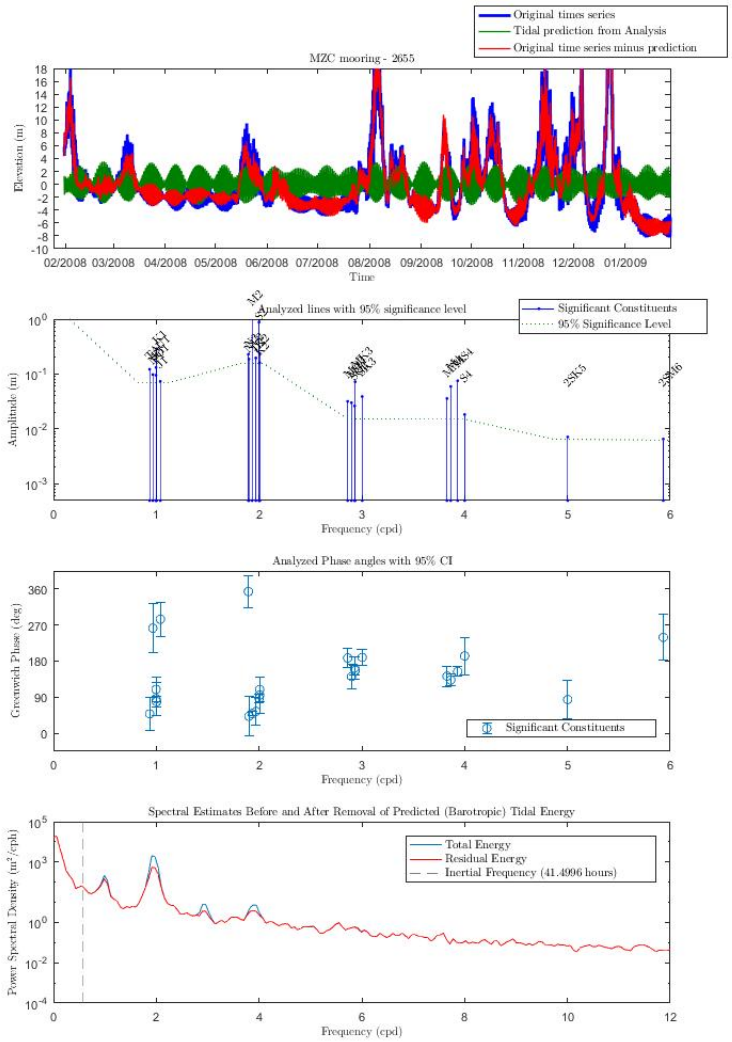

Figure 9: Results of T_TIDE analysis for lmc5a −2655.

Table 4: Difference in amplitude and phase between the deep sea measurements and altimeter data for the lmc5a−2655 location. Amplitude difference is in cm and phase difference is in degrees.

	K1	K2	M2	M4	N2	O1	P1	Q1	S2
Amplitude difference	22.67 ± 6.9	0.79 ± 15.7	51.39 ± 15.7	5.24 ± 1.5	3.33 ± 15.7	nvt	7.45 ± 6.9	nvt	26.25 ± 15.7
Phase difference	72.78 ± 12.33	20.67 ± 44.2	46.36 ± 5.65	130.22 ± 15.36	336.68 ± 40.78	nvt	80.70 ± 40.94	nvt	11.03 ± 10.23

3.2.4 Mooring lmc5a −3623

The measurements done at station 3623 show that the device measuring the data did not work well. Looking at Fig. 10 we see that the data after mid-October 2008 looks corrupted. The data before this date still looks alright, apart from one dip in the pressure in early September 2008, but this looks like it is only one instance so we can still perform harmonic analysis on this part.
Looking at Fig. 11, in the first plot delivered by the analysis we see that only one big peak is present. This is remarkable since the peaks in the results from 2655 are so heavily present, one would expect those peaks in this time series as well. Looking at the amplitudes, we see a lot of significant constituents, including a long period constituent in SSA. Furthermore we see here that M2 is once again the major constituent followed by S2. In the phase spectrum we see that most phase angles are grouped up for a few exceptions. In the energy spectrum we only see peaks at tidal frequencies. The energy spectrum also looks suspiciously smooth, this is because the data set used is shorter than the rest of the data sets. Finetuning of parameters used for calculating the PSD can make sure the spectrum looks less smooth, this is however not necessary for this research.

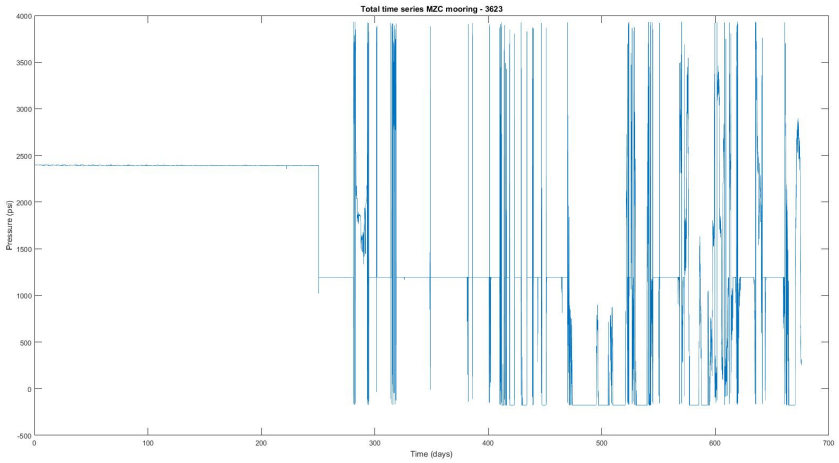

Figure 10: Total data collected by lmc5a −3623 the x-axis shows the time in days, where $t = 0$ corresponds to the time of first measurement.

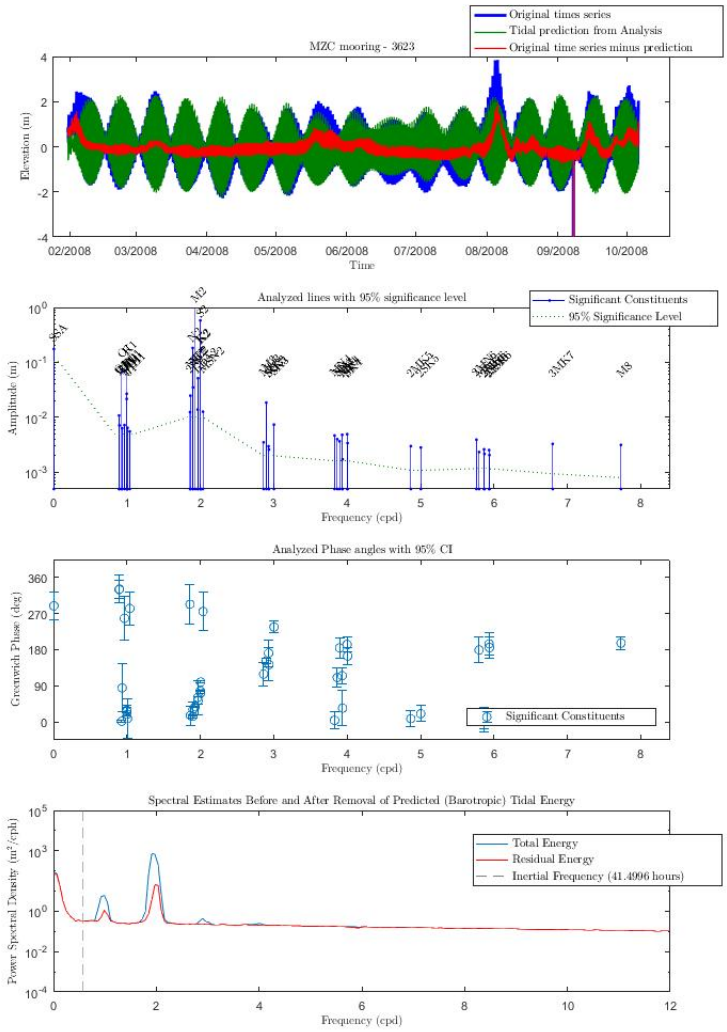

Figure 11: Results of T_TIDE analysis for lmc5a −3623.

Table 5: Difference in amplitude and phase between the deep sea measurements and altimeter data for the lmc5a−3623 location. Amplitude difference is in cm and phase difference is in degrees.

	K1	K2	M2	M4	N2	O1	P1	Q1	S2
Amplitude difference	1.43 ± 0.5	0.04 ± 1	1.33 ± 1	0.94 ± 0.2	0.97 ± 1	0.69 ± 0.5	0.42 ± 0.5	0.482 ± 0.5	3.431 ± 1
Phase difference	12.39 ± 3.27	2.35 ± 2.67	35.02 ± 0.52	108.05 ± 24.62	3.215 ± 3.21	355.86 ± 3.75	20.31 ± 10.9	6.35 ± 22.68	0.76 ± 0.99

3.2.5 Mooring lmc6 − 3624

Moving on to lmc6 − 3624. In the top plot of Fig. 12 we see two big peaks and a few smaller peaks. The plot for amplitudes shows what one would expect once again, with the biggest amplitudes in the diurnal and semidiurnal bands, and the frequency of significant constituents reaching 0.25 cph. One difference with the other sites is the presence of the MSM constituent, which seems to have a very big influence on the tides with an amplitude almost as big as that

of S2. Examining the phase angles, there is not much to say. Those phase angles in the same tidal bands seem to be grouped up, following the credo of smoothness. Looking at the energy spectrum, we see a small peak at the inertial frequency and bigger peaks at frequencies given to tidal constituents. What looks remarkable here is that the residual energy still shows really strong peaks at these tidal frequencies. It turns out these peaks are not exactly at the tidal frequencies but at the neighbouring frequencies. These peaks show that there still is indeed influence from internal tides.

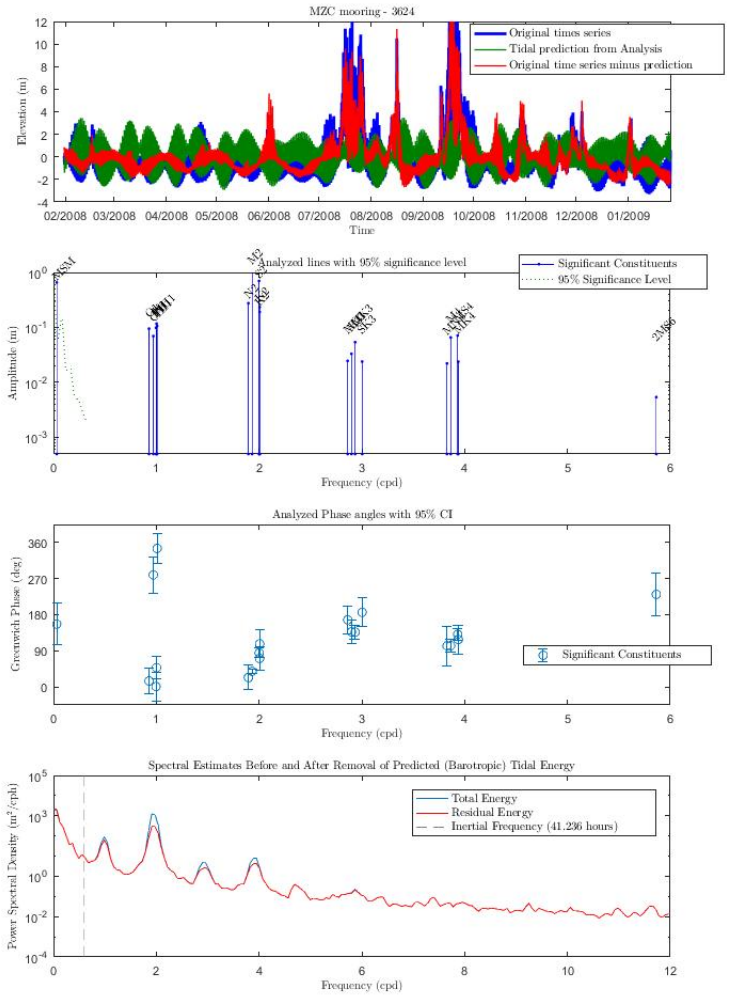

Figure 12: Results of T_TIDE analysis for lmc6.

Table 6: Difference in amplitude and phase between the deep sea measurements and altimeter data for the lmc6 location. Amplitude difference is in cm and phase difference is in degrees.

	K1	K2	M2	M4	N2	O1	P1	Q1	S2
Amplitude difference	4.84 ± 6.3	6.16 ± 14.4	15.77 ± 14.4	5.93 ± 1.8	8.09 ± 14.4	3.46 ± 6.3	7.50 ± 6.3	nvt	8.22 ± 14.4
Phase difference	38.07 ± 28	3.69 ± 28.34	2.87 ± 6.58	100.42 ± 16.68	6.00 ± 16.68	326.16 ± 32.83	8.24 ± 36.78	nvt	8.69 ± 11.74

3.2.6 Mooring lmc7 – 4347

The lmc7 – 4347 data, shown in Fig. 13 reveals big peaks located around early August and November 2008. The rest of the plots follow the general trend like the rest of the data so far, with main amplitudes in the diurnal and semidiurnal bands, phase angles grouped up following the credo of smoothness and peaks at the tidal bands in the energy spectrum.

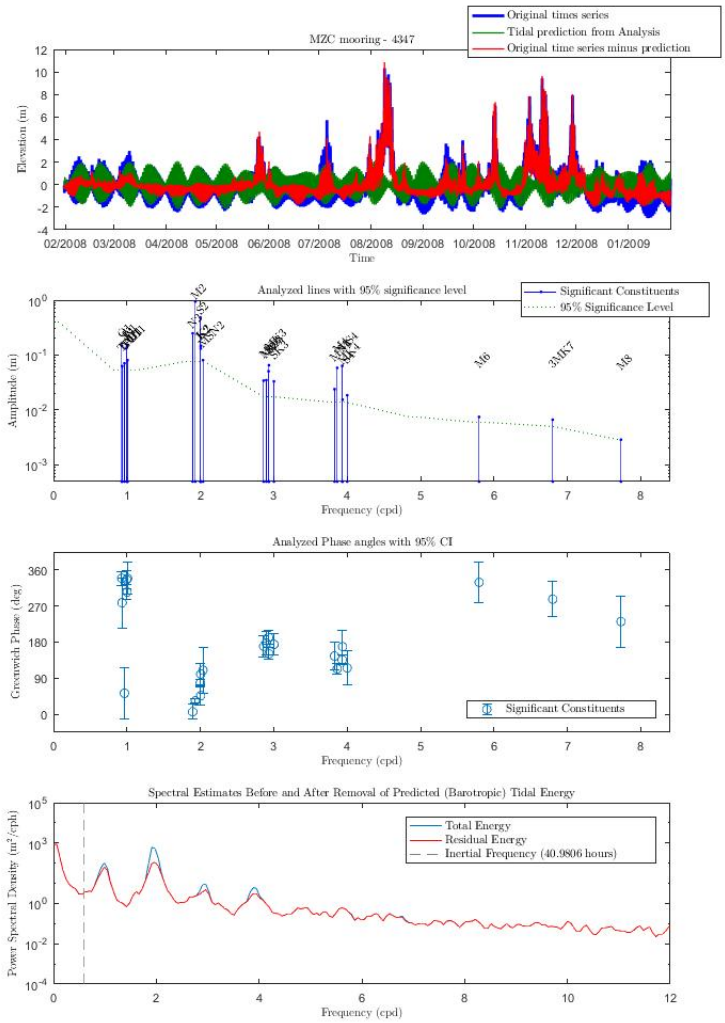

Figure 13: Results of T_TIDE analysis for lmc7.

Table 7: Difference in amplitude and phase between the deep sea measurements and altimeter data for the lmc7 location. Amplitude difference is in cm and phase difference is in degrees.

	K1	K2	M2	M4	N2	O1	P1	Q1	S2
Amplitude difference	7.56 ± 5.3	2.8 ± 7.8	19.85 ± 7.8	5.23 ± 1.4	5.26 ± 7.8	8.84 ± 5.3	11.2 ± 5.3	nvt	13.9 ± 7.8
Phase difference	291.06 ± 18.74	28.35 ± 24.54	2.49 ± 4.84	111.37 ± 14.21	11.18 ± 18.28	295.01 ± 17.56	325.73 ± 22.38	nvt	2.05 ± 9.15

3.2.7 Mooring lmc8 – 2672

The lmc8 – 2672, Fig. 14, shows no real peaks besides the tidal peaks in the time series. This means that this location gives a really clean look to the tides in this area. Looking at the amplitude and phase spectrum, we see amplitude peaks in the diurnal and semidiurnal band, with M2 and S2 being the biggest constituents. The phase angles look to be grouped up, following the credo of smoothness. Looking at the energy spectrum, we notice one thing different from the energy spectra from the other locations, namely an energy dip at the inertial frequency.

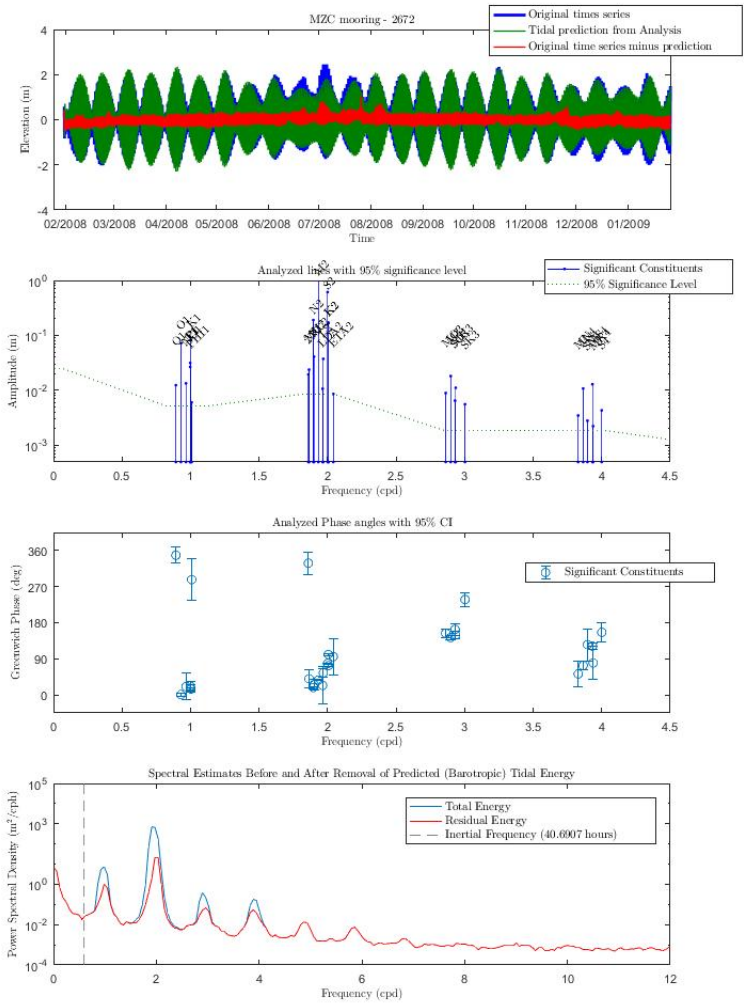

Figure 14: Results of T_TIDE analysis for lmc8.

Table 8: Difference in amplitude and phase between the deep sea measurements and altimeter data for the lmc8 location. Amplitude difference is in cm and phase difference is in degrees.

	K1	K2	M2	M4	N2	O1	P1	Q1	S2
Amplitude difference	0.55 ± 0.5	0.45 ± 0.9	2.29 ± 0.9	0.47 ± 0.2	0.9 ± 0.9	1.09 ± 0.5	0.167 ± 0.5	0.2 ± 0.5	1.75 ± 0.9
Phase difference	3.93 ± 3.37	2.13 ± 2.32	0.59 ± 0.45	1.78 ± 10.66	0.56 ± 2.66	3.29 ± 3.58	4.36 ± 11.18	322.42 ± 20.22	2.22 ± 0.8

3.2.8 Mooring lmctrap − 2959

In Fig. 15 we see the data collected by lmctrap−2959. First off, notice that the recording starts 14 months later than the recordings at the other locations. Also, the recording lasts for about nine months, which is three months shorter than the analysed data on other sites (except for the lmc5a−3623). Looking at the amplitude and phase spectrum we notice a lot more significant constituents compared to the other sites. Although there are a lot more significant constituents, M2 and S2 still are the main components to the tidal waves with the other main constituents from the diurnal and semidiurnal band also present. The phase spectrum looks very cluttered with this amount of significant constituents, but, with a few exceptions, the credo of smoothness still seems to be followed. Furhtermore, the energy spectrum shows no real surprises. With peaks at tidal frequencies, which are lowered, but still present, in the residual energy.

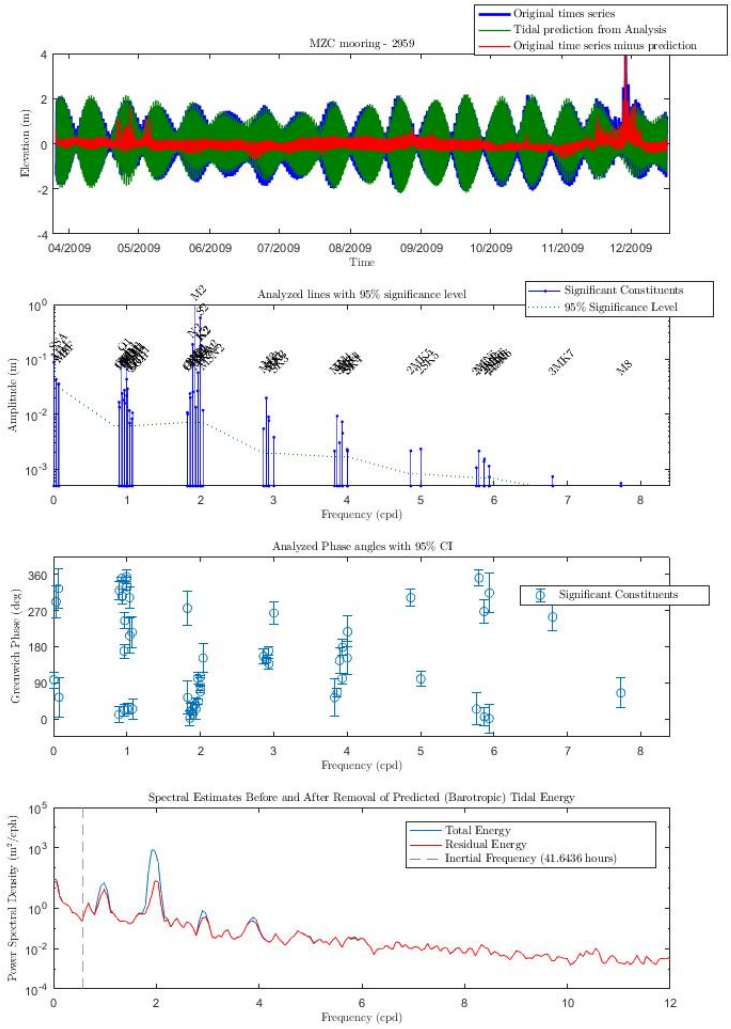

Figure 15: Results of T_TIDE analysis for lmctrap.

Table 9: Difference in amplitude and phase between the deep sea measurements and altimeter data for the lmctrap location. Amplitude difference is in cm and phase difference is in degrees.

	K1	K2	M2	M4	N2	O1	P1	Q1	S2
Amplitude difference	0.04 ± 0.6	0.167 ± 0.7	3.61 ± 0.7	0.25 ± 0.2	0.42 ± 0.7	2.22 ± 0.6	0.03 ± 0.6	0.08 ± 0.6	4.1 ± 0.7
Phase difference	342.71 ± 5.05	6.18 ± 2.04	0.35 ± 0.39	63.75 ± 10.79	4.53 ± 2.23	6.2 ± 3.92	350.54 ± 16.35	324.63 ± 19.06	6.66 ± 0.72

3.3 East Madagascar Current

3.3.1 EMC1

Looking at the plots in Fig. 16, showing the results from EMC1, we immediately see big differences with the data sets collected in the Mozambique Channel. The first plot shows the water elevation, however we do not see the standard high− and low tide, there is no clear

spring− and neap tide cycle. Also, the water elevation is lower than that in the Mozambique Channel. About a maximum of 1 m in the EMC, while approximately 2 m in the Mozambique Channel. This difference of lower water elevation is also seen in the amplitude spectrum. The biggest tidal constituent, M2, reaches near 0.15 m, while in the Mozambique Channel, M2 reaches amplitudes of over 1 m, so nearly ten times as big. Also, the amount of significant constituents that are not in the diurnal or semidiurnal band is lower than in the Mozambique Channel. That means the amplitude of these constituents is so small that they get lost in the noise of the measurements. Noticeable as well is the SSA constituent, with an amplitude nearly as big as S2. Analyzing the phase angles, we see that those in the diurnal band are not well grouped and therefore, we must conclude that they do not follow the credo of smoothness. Looking at the energy spectrum, we see once more what we already suspected. There is a lot less energy in total due to water elevation, with tidal peaks at the diurnal and semidiurnal bands.

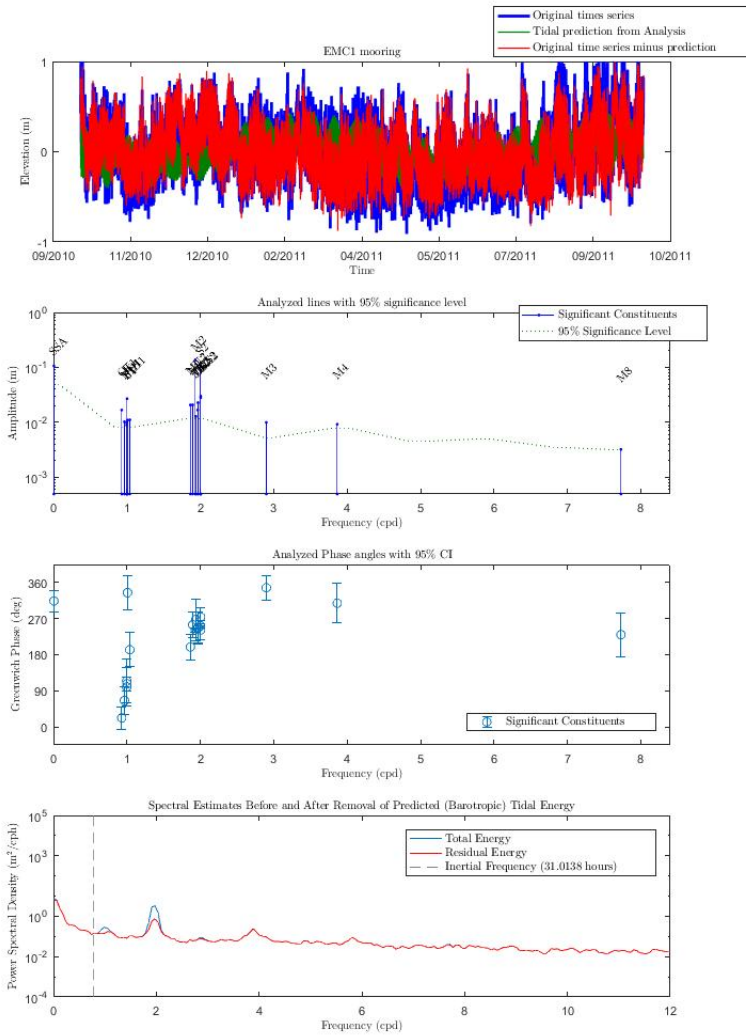

Figure 16: Results of T_TIDE analysis for EMC1.

Table 10: Difference in amplitude and phase between the deep sea measurements and altimeter data for the EMC1 location. Amplitude difference is in cm and phase difference is in degrees.

	K1	K2	M2	M4	N2	O1	P1	Q1	S2
Amplitude difference	0.37 ± 0.8	0.85 ± 1.2	4.19 ± 1.2	0.57 ± 0.8	0.32 ± 1.2	0.19 ± 0.8	0.04 ± 0.8	nvt	4.19 ± 1.2
Phase difference	18.47 ± 17.54	15.25 ± 23.96	19.22 ± 4.9	19.19 ± 48.97	16.2 ± 32.2	1.74 ± 28.17	7.50 ± 53.54	nvt	9.74 ± 6.11

3.3.2 EMC3

Fig. 17 shows the results from the analysis of the data collected by EMC3. Here, we see the same kind of results as collected by EMC1. Again, in the times series we see a lack of influence by spring− and neap tide. In the amplitude spectrum we see most significant constituents in the diurnal and semidiurnal bands, with M2 and S2 being the most dominant one. There is also a long period constituent present with MSM, which is the third biggest constituent at this location. The phase angles also show the same pattern as the EMC1 data. With the phase angles in the diurnal band being cluttered, while those in the semidiurnal band look to be grouped. Therefore, the credo of smoothness is followed for the semidiurnal components, but not followed for the diurnal ones. Lastly, the energy spectrum shows us nothing new, with once again peaks at the diurnal and semidiurnal bands, which are remarkably lower in the residual energy.

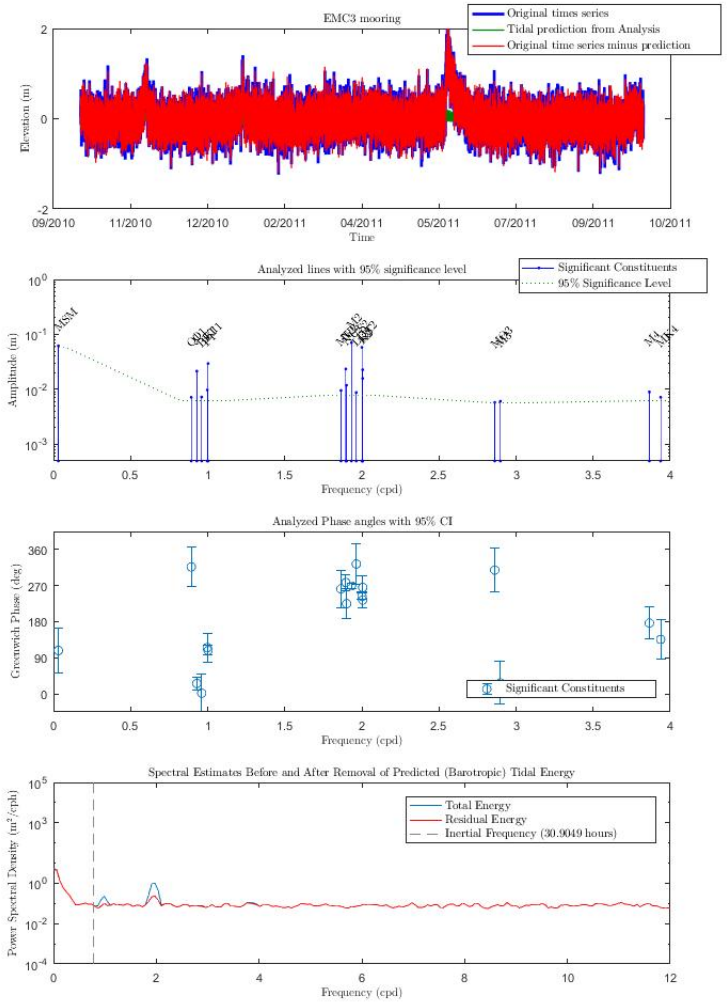

Figure 17: Results of T_TIDE analysis for EMC3.

Table 11: Difference in amplitude and phase between the deep sea measurements and altimeter data for the EMC3 location. Amplitude difference is in cm and phase difference is in degrees.

	K1	K2	M2	M4	N2	O1	P1	Q1	S2
Amplitude difference	0.16 ± 0.6	0.29 ± 0.8	2.26 ± 0.8	0.54 ± 0.6	0.19 ± 0.8	5.76 ± 0.6	0.04 ± 0.6	0.03 ± 0.6	1.31 ± 0.8
Phase difference	15.19 ± 11.97	22.68 ± 19.95	6.19 ± 6.42	151.87 ± 39.45	4.03 ± 19.23	4.82 ± 16.46	4.18 ± 36.54	38.81 ± 48.98	18.55 ± 7.83

4 Conclusion and Discussion

The results gathered in this research give an overview of the behaviour of the tides in both the Mozambique Channel and near Eastern Madagascar. The differences in both amplitude and phase between these two location show once more the influence of bathymetry to the

behaviour of tides. Comparing the results to altimeter data we still see relatively big differences in both amplitude and phase for some of the biggest constituents. Improving the results obtained from the deep sea measurements may make these differences smaller. One way to improve the results is by considering longer data sets. For this research, only one year of data was used. Averaging over multiple years of data gives a better view of the overall behaviour of tides since constituents with periods over a year are then also accounted for. Second, since none of the Mozambique Channel measurements were true bottom measurements there are fluctuations due to internal tides and cable movement which appear in the measurements as sea surface fluctuations. To get a better view of the tides, there should be made adjustments, so these fluctuations do not appear in the harmonic analysis. Furthermore, as discussed in chapter 3.1, there is a time drift present in the data sets from the Mozambique Channel. It is clear that this time drift affects the results obtained. Therefore to get more precise results, this time drift should be accounted for. Although this only gives an error of about 1.39 degrees and 2.5 cm to the phase angle and amplitude respectively. We may conclude from this that the time drift is only relevant for those constituents where the amplitudes, phase angles and their errors fall in this order of magnitude. Lastly, the errors in altimeter data must also be accounted for. Since this is not done in this research.
Once these improvements to the results have been made we truly have a good view of how the tides behave in this area. Only then this data can be used to research the internal tides in this area and to contribute to test models of the tides.

References

[1] D. Cartwright, *Tides: A Scientific History* (Cambridge University Press, 2000).

[2] R. D. Ray, Journal of Geophysical Research: Oceans **118**, 4570 (2013), ISSN 2169-9291, URL `http://dx.doi.org/10.1002/jgrc.20336`.

[3] *Tides and water levels*, URL `http://oceanservice.noaa.gov/education/kits/tides/lessons/tides_tutorial.pdf`.

[4] G. Platzman, *Ocean tides and related waves*, Published in Mathematical methods in the geophysical sciences, part 2: inverse problems, dynamo theory and tides (ed. W. H. Reid), pp. 239292. Amer. Math. Soc.

[5] W. Munk and D. Cartwright, *Tidal spectroscopy and prediction* (1966).

[6] J. Ullgren, H. van Aken, H. Ridderinkhof, and W. de Ruijter, Deep Sea Research Part I: Oceanographic Research Papers **69**, 36 (2012), ISSN 0967-0637, URL `http://www.sciencedirect.com/science/article/pii/S0967063712001446`.

[7] L. Ponsoni, B. Aguiar-Gonzlez, H. Ridderinkhof, and L. Maas, Journal of Physical Oceanography **46**, 1045 (2016), `http://dx.doi.org/10.1175/JPO-D-15-0154.1`, URL `http://dx.doi.org/10.1175/JPO-D-15-0154.1`.

[8] *Got-e: the goddard/grenoble ocean tide model, extended*, URL `http://web.cecs.pdx.edu/%7Ezaron/pub/GOT-e.html`.

[9] *Mathworks documantation: hann*, URL `https://nl.mathworks.com/help/signal/ref/hann.html`.

[10] L. Maas, *Wave Attractors, Lecture Notes*, IMAU (2015).

[11] R. Pawlowicz, B. Beardsley, and S. Lentz, Computers and Geosciences **28**, 929 (2002), ISSN 0098-3004, URL `http://www.sciencedirect.com/science/article/pii/S0098300402000134`.

A Data collected by deep sea measurements

Here is presented the data on all the amplitudes and phase angles as calculated by T_TIDE from the deep sea measurements.

Tide	Amplitde	Amp error	Phase	Phase error
NO1	0.11345	0.07494	90	57.96
P1	0.16934	0.07494	46.55	25.53
P1	0.08	0.07494	77.05	54.03
K1	0.24175	0.07494	69.98	16.28
J1	0.1143	0.07494	42.8	30.24
N2	0.29895	0.09677	52.84	19.04
M2	1.38527	0.09677	40.69	4.12
MKS2	0.11275	0.09677	282.17	40.63
LDA2	0.1193	0.09677	6.27	48.08
L2	0.11421	0.09677	121.37	37.34
S2	0.81156	0.09677	79.73	6.82
K2	0.2199	0.09677	63.93	20.26
K2	0.22087	0.09677	102.13	20.17
MSN2	0.11488	0.09677	27.63	50.94
MO3	0.02163	0.01755	136.28	41.54
M3	0.02652	0.01755	136.94	39.58
SO3	0.02223	0.01755	172.83	39.2
MK3	0.03704	0.01755	129.91	25.62
SK3	0.02006	0.01755	180.3	45.88
MN4	0.03008	0.01648	170.21	33.17
M4	0.03881	0.01648	101.37	25.79
MS4	0.03893	0.01648	146.1	24.93
S4	0.01872	0.01648	219.29	50.27

Figure 18: Amplitudes (m) and phase angles (degree) collected at lmc4. Also includes errors.

Tide	Amplitde	Amp error	Phase	Phase error
SSA	0.21352	0.15943	119.04	42.78
Q1	0.01578	0.01162	356.84	35.76
O1	0.06629	0.01162	7.83	8.72
BET1	0.01417	0.01162	356.23	39.78
CHI1	0.01275	0.01162	73.47	45.2
P1	0.01854	0.01162	77.18	36.18
P1	0.02817	0.01162	36.44	23.8
K1	0.08512	0.01162	29.37	7.17
PHI1	0.02302	0.01162	182.75	31.16
J1	0.01424	0.01162	12.98	37.67
MU2	0.02505	0.01877	46.01	44.58
N2	0.17785	0.01877	26.26	6.21
NU2	0.05624	0.01877	37.66	19.73
M2	1.15989	0.01877	38.25	0.96
MKS2	0.0261	0.01877	186.92	34.02
L2	0.03249	0.01877	83.93	25.5
S2	0.62429	0.01877	77.73	1.72
K2	0.17257	0.01877	76.66	5
K2	0.1699	0.01877	100.13	5.08
MO3	0.00994	0.00273	155.79	14.05
M3	0.02111	0.00273	148.44	7.73
SO3	0.00624	0.00273	189.2	21.69
MK3	0.00977	0.00273	152.66	15.11
SK3	0.00604	0.00273	247.07	23.67
M4	0.00569	0.00201	82.96	21.44
SN4	0.00403	0.00201	167.47	29.27
MS4	0.00914	0.00201	129.07	12.95
2MN6	0.00116	0.00091	53.7	48.8
2MS6	0.00154	0.00091	248.01	35.83
2MK6	0.00104	0.00091	347.25	42.65

Figure 19: Amplitudes (m) and phase angles (degree) collected at lmc5. Also includes errors.

Tide	Amplitde	Amp error	Phase	Phase error
TAU1	0.12241	0.06903	48.45	42.19
NO1	0.09815	0.06903	262.27	61.39
P1	0.13211	0.06903	109.49	30.14
P1	0.09545	0.06903	86.11	41.72
K1	0.28842	0.06903	79.04	12.57
J1	0.074	0.06903	284.66	43.11
N2	0.22983	0.15697	353.72	40.17
NU2	0.18765	0.15697	42.58	49.44
M2	1.63777	0.15697	48.98	5.65
L2	0.1967	0.15697	54.44	35.17
S2	0.87793	0.15697	86.93	10.23
K2	0.16111	0.15697	95.45	44.85
K2	0.23893	0.15697	109.33	30.24
MO3	0.03197	0.01531	187.72	24.51
M3	0.0302	0.01531	141.3	30.3
SO3	0.02635	0.01531	162.93	28.84
MK3	0.07254	0.01531	156.73	11.41
SK3	0.03913	0.01531	189.29	20.51
MN4	0.036	0.01498	142.44	25.2
M4	0.05958	0.01498	132.89	15.27
MS4	0.07564	0.01498	154.12	11.67
S4	0.01841	0.01498	192.94	46.49
2SK5	0.00719	0.00652	84.14	47.48
2SM6	0.00657	0.00634	239.3	56.75

Figure 20: Amplitudes (m) and phase angles (degree) collected at lmc5a - 2655. Also includes errors.

Tide	Amplitde	Amp error	Phase	Phase error
SSA	0.17547	0.10389	289.29	33.92
Q1	0.01085	0.00509	329.97	22.68
RHO1	0.00717	0.00509	331.02	34.77
O1	0.06714	0.00509	1.5	3.75
TAU1	0.00638	0.00509	84.84	59.79
NO1	0.00727	0.00509	258.2	53.91
P1	0.0217	0.00509	29.24	13.53
P1	0.02694	0.00509	25.93	10.9
K1	0.08139	0.00509	18.86	3.27
PHI1	0.00647	0.00509	8.2	48.33
J1	0.00557	0.00509	282.91	42.2
2N2	0.01252	0.01001	293.4	49.77
MU2	0.02486	0.01001	15.92	23.99
N2	0.18335	0.01001	14.03	3.21
NU2	0.03514	0.01001	31.64	16.86
M2	1.1351	0.01001	37.62	0.52
LDA2	0.01387	0.01001	61.05	42.86
L2	0.05168	0.01001	52.99	8.72
S2	0.58094	0.01001	76.85	0.99
K2	0.17099	0.01001	72.38	2.67
K2	0.1581	0.01001	99.25	2.89
MSN2	0.01272	0.01001	275.28	47.69
MO3	0.00353	0.002	119.37	28.99
M3	0.0186	0.002	152.13	6.46
SO3	0.00299	0.002	171.64	33.11
MK3	0.00261	0.002	143.05	41.47
SK3	0.0074	0.002	236.52	14.15
MN4	0.0047	0.00163	3.97	21.06
M4	0.00403	0.00163	110.65	24.64
SN4	0.00369	0.00163	184.3	26.01
MS4	0.00484	0.00163	115.3	19.9
MK4	0.00174	0.00163	34.58	44.2
S4	0.00497	0.00163	193.1	18.77
SK4	0.00341	0.00163	164.32	21.81
2MK5	0.00301	0.00109	8.13	20.25
2SK5	0.00284	0.00109	20.5	20.12
2MN6	0.00394	0.00117	13.48	18.6
M6	0.00235	0.00117	179.4	31.27
2MS6	0.00263	0.00117	9.51	27.07
2MK6	0.00217	0.00117	2.27	26.14
2SM6	0.00255	0.00117	194.69	27.07
MSK6	0.00207	0.00117	185.44	26.57
3MK7	0.0033	0.00094	8.96	16.42
M8	0.00316	0.0008	196.76	16.44

Figure 21: Amplitudes (m) and phase angles (degree) collected at lmc5a - 3623. Also includes errors.

Tide	Amplitde	Amp error	Phase	Phase error
MSM	0.65857	0.60486	156.84	52.62
O1	0.09495	0.06271	14.76	32.83
CHI1	0.06961	0.06271	279.17	44.67
P1	0.09835	0.06271	0.67	36.78
K1	0.1176	0.06271	47.96	28
PHI1	0.10629	0.06271	345.26	36.42
N2	0.27573	0.14399	23.24	30.72
M2	1.29126	0.14399	38.95	6.58
S2	0.70142	0.14399	84.79	11.74
K2	0.23389	0.14399	70.95	28.34
K2	0.19089	0.14399	107.19	34.72
MO3	0.02465	0.01654	167.31	34.34
M3	0.03323	0.01654	137.11	29.76
MK3	0.05398	0.01654	136.51	16.56
SK3	0.02398	0.01654	186.1	36.16
MN4	0.02221	0.01806	102.56	49.25
M4	0.06577	0.01806	102.91	16.68
MS4	0.07124	0.01806	131.02	14.94
MK4	0.02389	0.01806	118.27	35.84
2MS6	0.0054	0.00468	230.7	52.62

Figure 22: Amplitudes (m) and phase angles (degree) collected at lmc6. Also includes errors.

Tide	Amplitde	Amp error	Phase	Phase error
O1	0.14915	0.05268	339.04	17.56
TAU1	0.06295	0.05268	278.41	62.54
NO1	0.07106	0.05268	52.39	64.36
P1	0.13581	0.05268	335.35	22.38
K1	0.14763	0.05268	304.79	18.74
PHI1	0.08084	0.05268	339.08	40.22
N2	0.2495	0.07753	6.22	18.28
M2	0.94466	0.07753	33.67	4.84
S2	0.48482	0.07753	78.09	9.15
K2	0.14542	0.07753	46.3	24.54
K2	0.13194	0.07753	100.49	27.05
MSN2	0.08093	0.07753	109.92	57.94
MO3	0.03429	0.01745	169.89	26.06
M3	0.03502	0.01745	177.45	29.8
SO3	0.05087	0.01745	192.21	17.03
MK3	0.06543	0.01745	150.95	14.42
SK3	0.03329	0.01745	174.25	27.48
MN4	0.02397	0.01372	145.25	34.65
M4	0.05862	0.01372	113.27	14.21
MS4	0.06362	0.01372	135.77	12.7
MK4	0.01544	0.01372	168.47	42.1
S4	0.0186	0.01372	115.61	42.13
M6	0.0075	0.00592	329.17	49.4
3MK7	0.00668	0.00505	287.3	43.33
M8	0.00288	0.00284	231.42	63.5

Figure 23: Amplitudes (m) and phase angles (degree) collected at lmc7. Also includes errors.

Tide	Amplitde	Amp error	Phase	Phase error
Q1	0.01248	0.00519	348.36	20.22
O1	0.07206	0.00519	0.8	3.58
NO1	0.01346	0.00519	20.81	33.37
P1	0.03167	0.00519	16.08	9.45
P1	0.02678	0.00519	21.87	11.18
K1	0.08092	0.00519	14.8	3.37
PHI1	0.00607	0.00519	287.42	52.76
2N2	0.01956	0.00862	328.4	27.49
MU2	0.02388	0.00862	40.23	21.47
N2	0.19075	0.00862	18.59	2.66
NU2	0.04114	0.00862	25.61	12.38
M2	1.13161	0.00862	37.15	0.45
LDA2	0.01075	0.00862	23.81	47.49
L2	0.03756	0.00862	55.09	10.11
S2	0.61379	0.00862	78.38	0.8
K2	0.17062	0.00862	72.91	2.32
K2	0.16704	0.00862	100.78	2.37
ETA2	0.00863	0.00862	95.49	44.67
MO3	0.00897	0.00184	153.73	10.5
M3	0.01826	0.00184	143.11	6.03
SO3	0.00653	0.00184	163.29	14
MK3	0.01118	0.00184	149.19	8.9
SK3	0.00561	0.00184	237.81	17.19
MN4	0.0035	0.0019	52.28	32.98
M4	0.01086	0.0019	73.29	10.66
SN4	0.00281	0.0019	125.15	39.78
MS4	0.01298	0.0019	121.76	8.64
MK4	0.00224	0.0019	79.88	40.3
S4	0.00435	0.0019	156.06	25.01

Figure 24: Amplitudes (m) and phase angles (degree) collected at lmc8. Also includes errors.

Tide	Amplitde	Amp error	Phase	Phase error
SSA	0.08805	0.03081	97.38	20.05
MM	0.04372	0.03081	292.05	40.37
MSF	0.03557	0.03081	325.26	49.62
MF	0.03583	0.03081	53.94	49.26
Q1	0.01669	0.00625	10.87	19.06
RHO1	0.0135	0.00625	320.13	23.27
O1	0.08241	0.00625	350.32	3.92
TAU1	0.02408	0.00625	305.46	17.74
BET1	0.01825	0.00625	168.92	17.37
NO1	0.02752	0.00625	21.97	14
CHI1	0.01597	0.00625	245.05	20.1
P1	0.0437	0.00625	329.74	8.23
P1	0.022	0.00625	354.39	16.35
K1	0.06647	0.00625	347.32	5.05
PHI1	0.02928	0.00625	25.18	12.93
THE1	0.01176	0.00625	302.3	27.48
J1	0.00697	0.00625	207.1	43.8
SO1	0.00839	0.00625	215.8	38.45
OO1	0.01071	0.00625	25.14	25.09
OQ2	0.01088	0.00716	275.94	41.37
EPS2	0.01011	0.00716	53.54	42.5
2N2	0.02393	0.00716	2.27	18.44
MU2	0.02023	0.00716	18.63	20.81
N2	0.18795	0.00716	12.79	2.23
NU2	0.02565	0.00716	25.36	16.4
M2	1.08544	0.00716	36.4	0.39
MKS2	0.01355	0.00716	24.7	26.5
LDA2	0.0268	0.00716	101.59	15.65
L2	0.05765	0.00716	43.66	6.22
S2	0.57227	0.00716	82.77	0.72
K2	0.17259	0.00716	68.63	2.04
K2	0.15574	0.00716	105.17	2.26
MSN2	0.0119	0.00716	151.81	35.94
MO3	0.0055	0.00197	156.31	18.85
M3	0.01989	0.00197	146.29	5.83
SO3	0.00903	0.00197	169.67	11.26
MK3	0.00774	0.00197	137.5	13.94
SK3	0.00385	0.00197	263.66	27.49
MN4	0.00216	0.0017	53.23	46.96
M4	0.00936	0.0017	66.27	10.79
SN4	0.00306	0.0017	145.39	32.47
MS4	0.00736	0.0017	100.94	13.46
MK4	0.00454	0.0017	178.66	18.73
S4	0.00231	0.0017	151.92	42
SK4	0.00216	0.0017	217.31	38.61
2MK5	0.00218	0.00082	302.1	21.08
2SK5	0.00236	0.00082	99.7	18.7
2MN6	0.00107	0.00071	24.55	39.99
M6	0.00216	0.00071	351.34	19.79
2MS6	0.00139	0.00071	267.81	30.13
2MK6	0.00155	0.00071	5.34	23.28
2SM6	0.00115	0.00071	0.77	35.81
MSK6	0.00073	0.00071	313.86	48.66
3MK7	0.00074	0.00044	254.1	33.64
M8	0.00056	0.00034	64.77	37.64

Figure 25: Amplitudes (m) and phase angles (degree) collected at lmctrap. Also includes errors.

Tide	Amplitde	Amp error	Phase	Phase error
SSA	0.10689	0.04993	313.95	26.76
O1	0.01683	0.00835	22.33	28.17
NO1	0.01029	0.00835	65.66	33.93
P1	0.00989	0.00835	99.64	48.4
P1	0.00894	0.00835	114.49	53.54
K1	0.02702	0.00835	107.42	17.54
PHI1	0.01103	0.00835	334.57	41.57
J1	0.01113	0.00835	192.5	42.65
MU2	0.02076	0.01179	199.5	32.38
N2	0.02087	0.01179	254.51	32.2
M2	0.13751	0.01179	242.13	4.9
MKS2	0.0129	0.01179	267.61	52.14
LDA2	0.01681	0.01179	245.72	40.08
L2	0.0229	0.01179	247.69	37.64
S2	0.11062	0.01179	251.67	6.11
K2	0.02815	0.01179	241.81	23.96
K2	0.0301	0.01179	274.07	22.41
M3	0.01002	0.00533	346.94	30.33
M4	0.00927	0.00797	308.54	48.97
M8	0.00325	0.00315	229.93	54.91

Figure 26: Amplitudes (m) and phase angles (degree) collected at EMC1. Also includes errors.

Tide	Amplitde	Amp error	Phase	Phase error
MSM	0.06225	0.05965	108.28	54.9
Q1	0.0072	0.00624	316.78	48.98
O1	0.02153	0.00624	26	16.46
BET1	0.00727	0.00624	1.92	48.43
P1	0.00979	0.00624	115.33	36.54
K1	0.0296	0.00624	108.26	11.97
MU2	0.0096	0.00796	261.78	47.27
N2	0.02357	0.00796	277.49	19.23
NU2	0.01193	0.00796	224.84	37.94
M2	0.07085	0.00796	269.37	6.42
LDA2	0.00879	0.00796	323.92	51.68
S2	0.05823	0.00796	243.07	7.83
K2	0.02282	0.00796	234.3	19.95
K2	0.01585	0.00796	265.47	28.72
MO3	0.0058	0.00568	308.7	55.43
M3	0.00611	0.00568	27.19	53.04
M4	0.00901	0.00624	176.71	39.45
MK4	0.00723	0.00624	135.8	49.22

Figure 27: Amplitudes (m) and phase angles (degree) collected at EMC3. Also includes errors.

B Data collected by altimeter satellites

Here is presented the data on amplitudes and phase angles computed from data collected by altimeter satellites. There are two subsections here. Subsection B.1 shows the altimeter data in figures while subsection B.2 shows this data in tables.

B.1 Altimeter data in figures

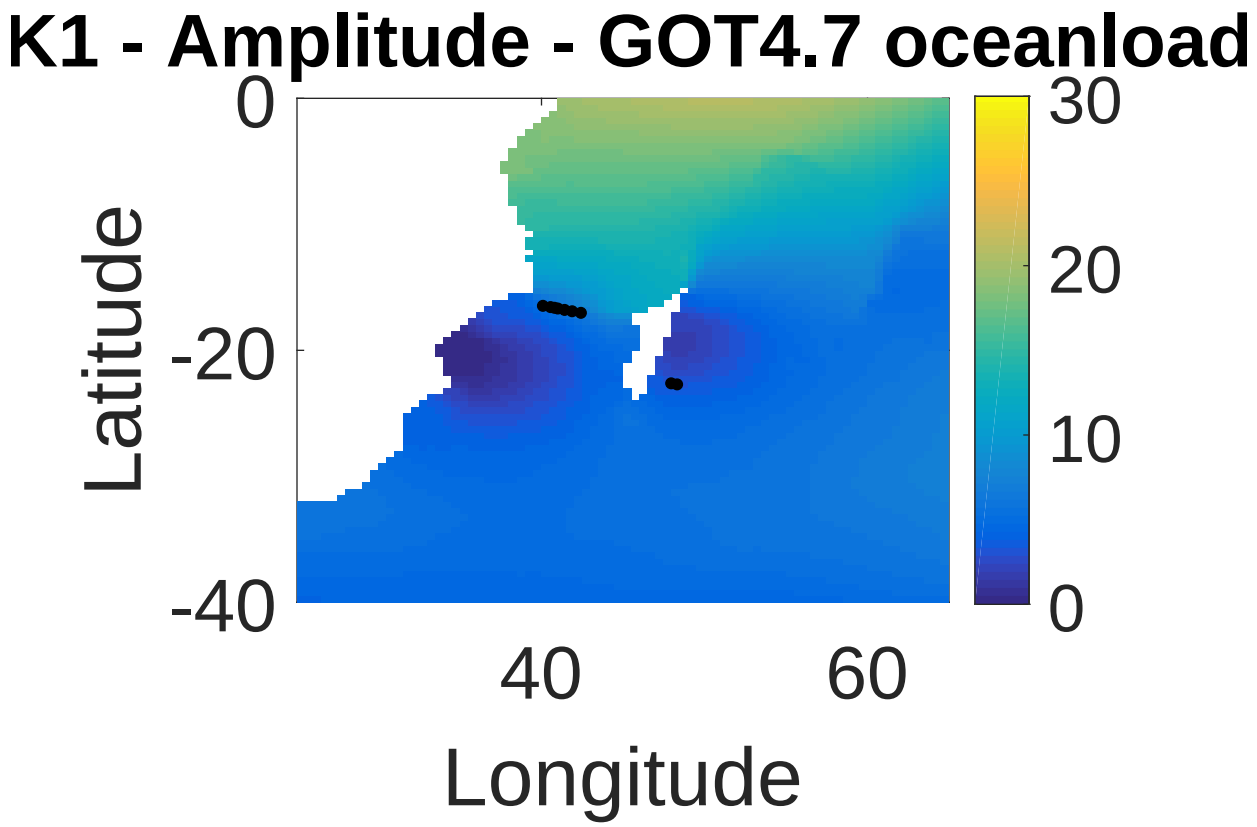

Figure 28: Amplitude for the K1 constituent. Black points indicate the locations of the measurement stations.

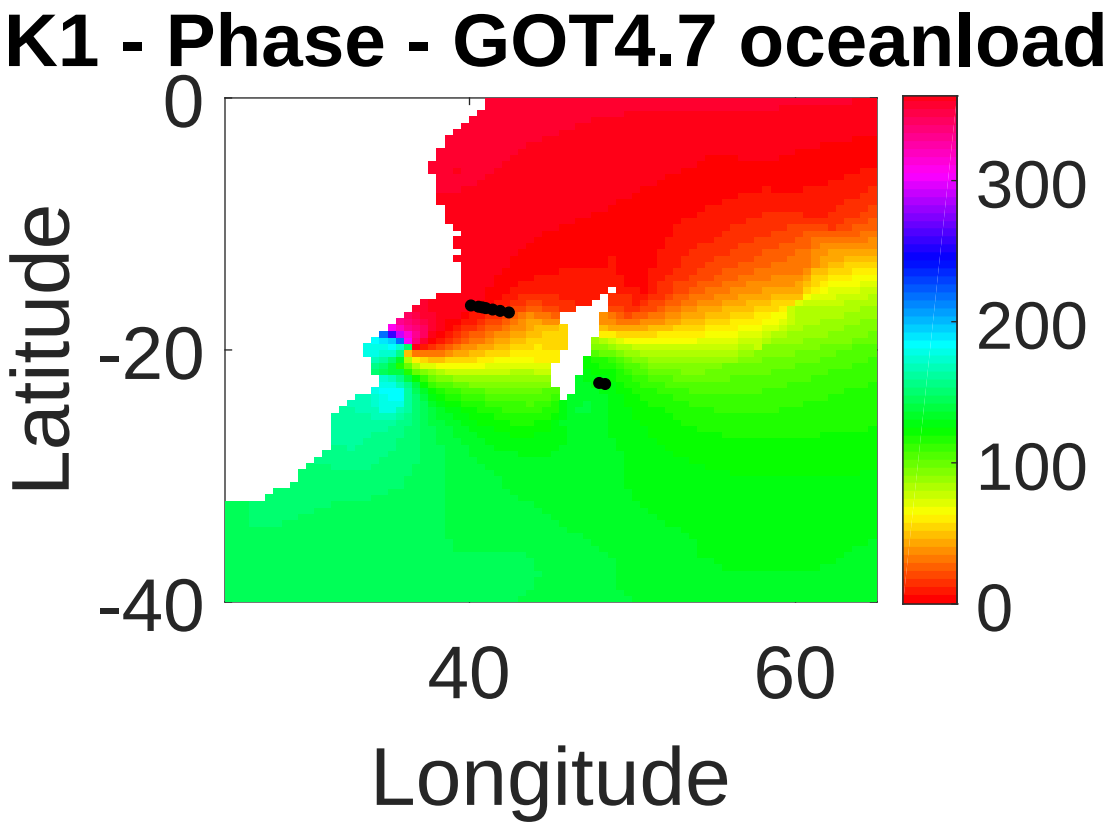

Figure 29: Phase for the K1 constituent. Black points indicate the locations of the measurement stations.

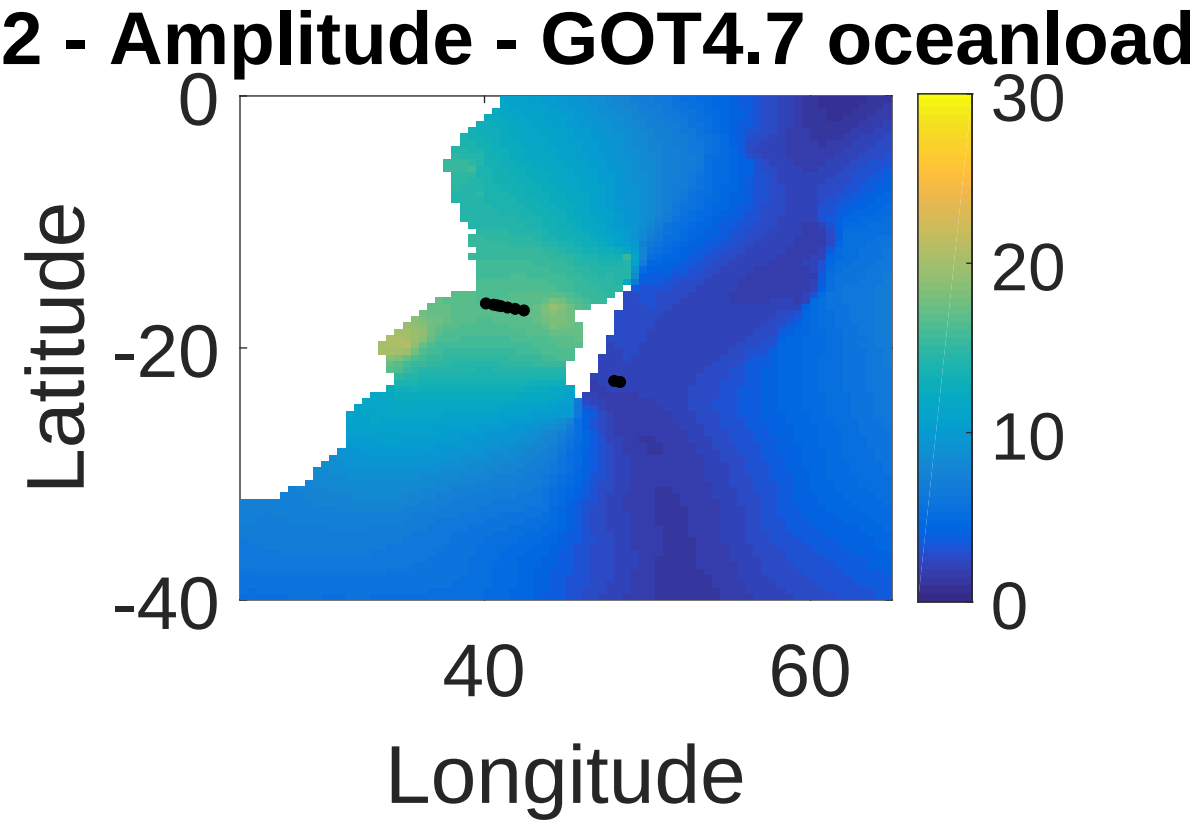

Figure 30: Amplitude for the K2 constituent. Black points indicate the locations of the measurement stations.

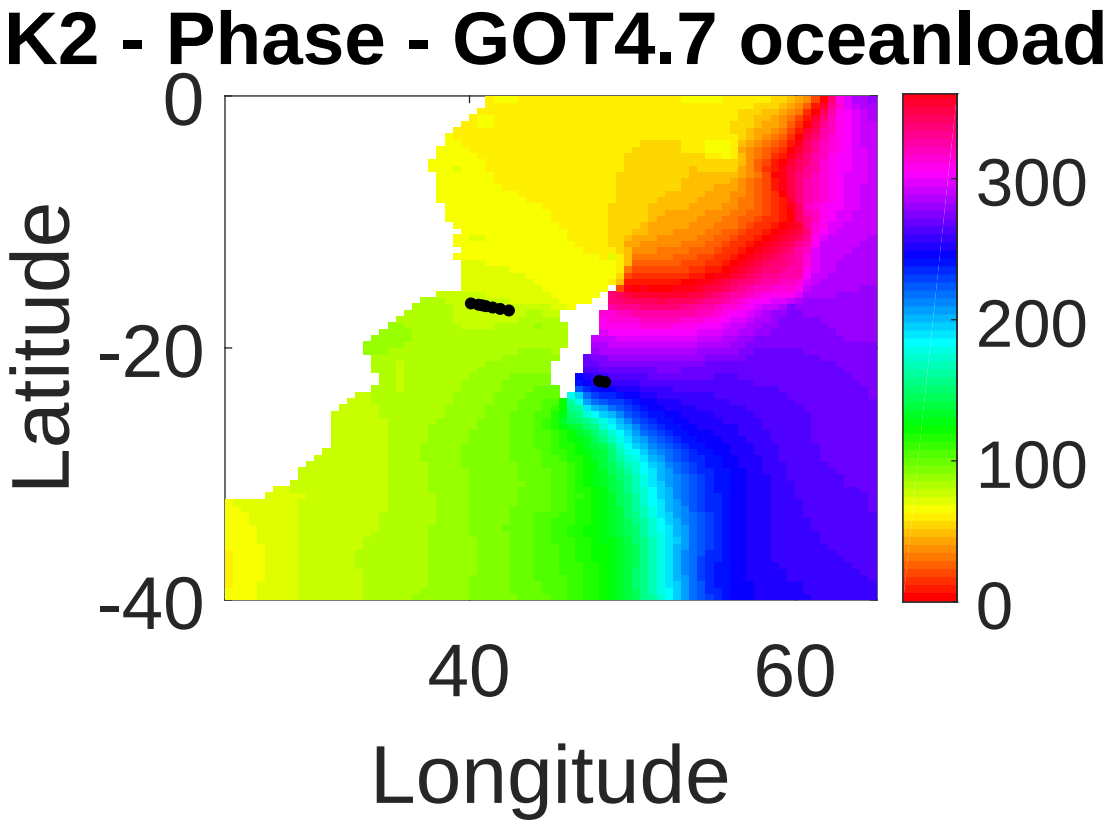

Figure 31: Phase for the K2 constituent. Black points indicate the locations of the measurement stations.

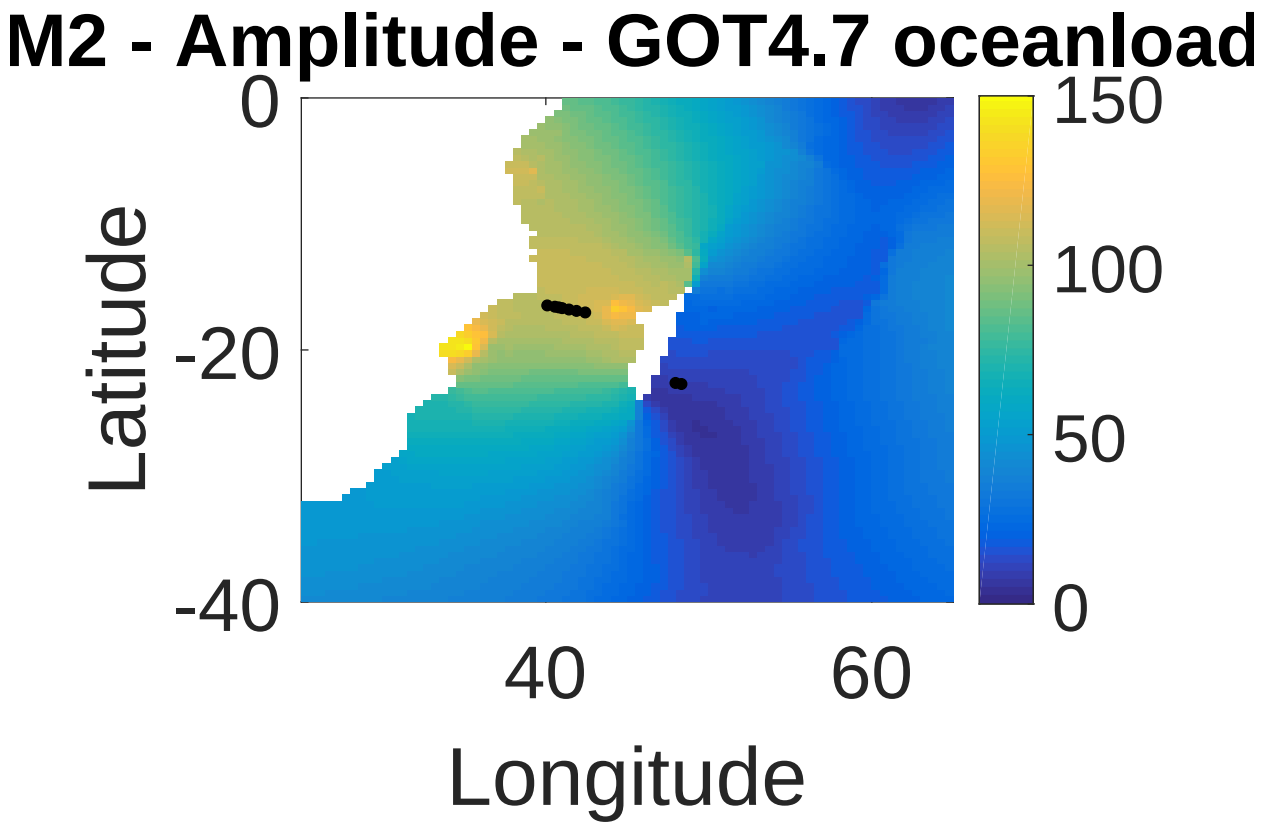

Figure 32: Amplitude for the M2 constituent. Black points indicate the locations of the measurement stations.

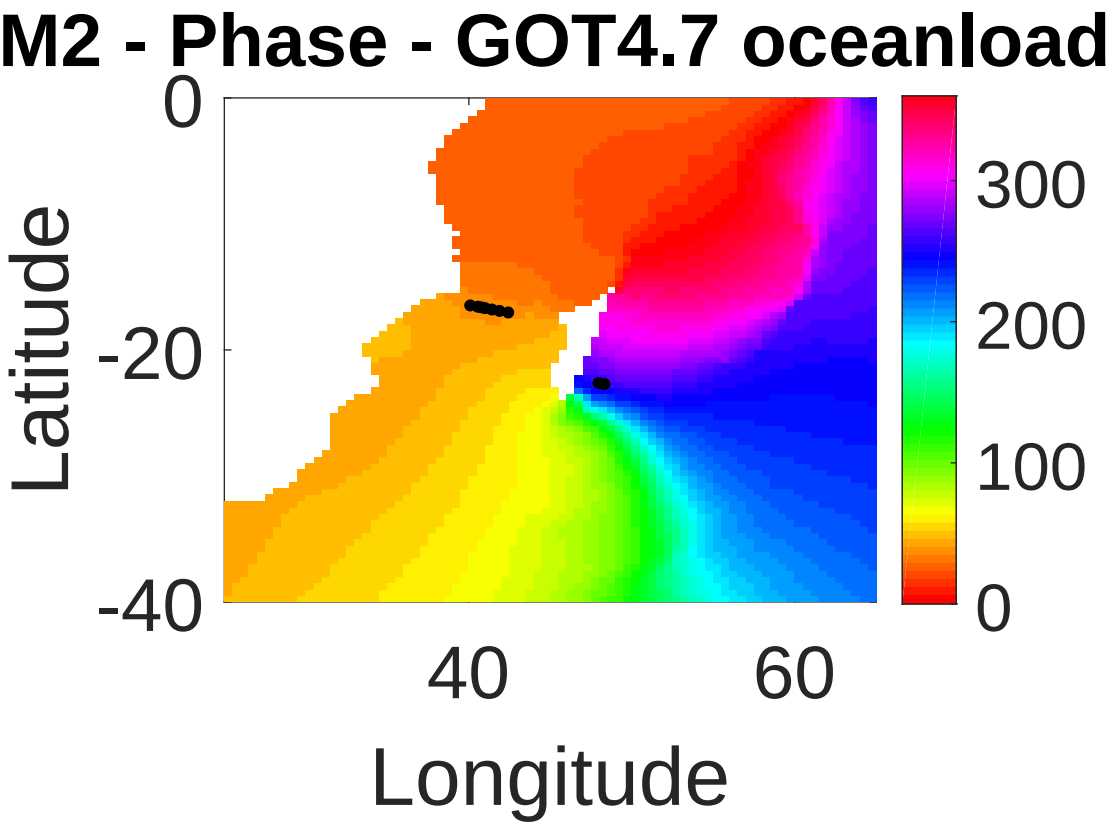

Figure 33: Phase for the M2 constituent. Black points indicate the locations of the measurement stations.

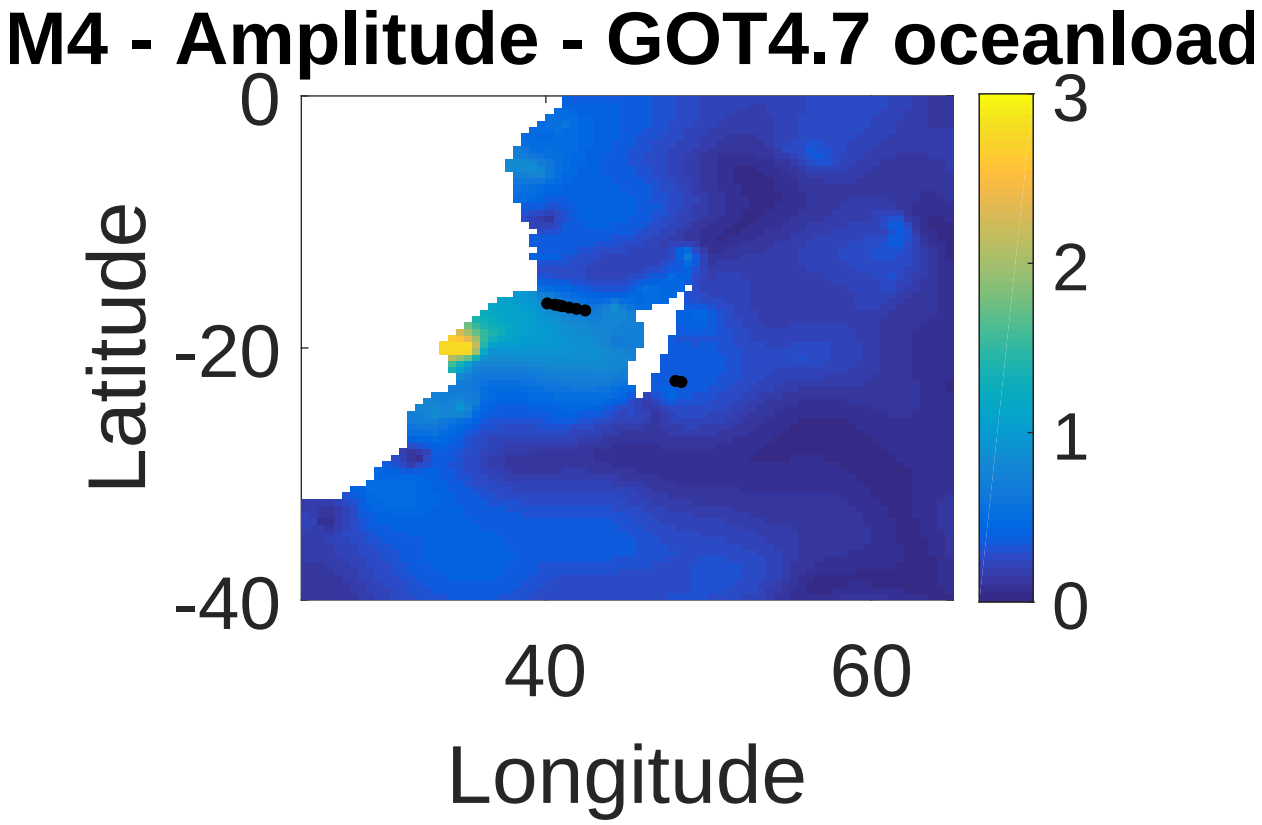

Figure 34: Amplitude for the M4 constituent. Black points indicate the locations of the measurement stations.

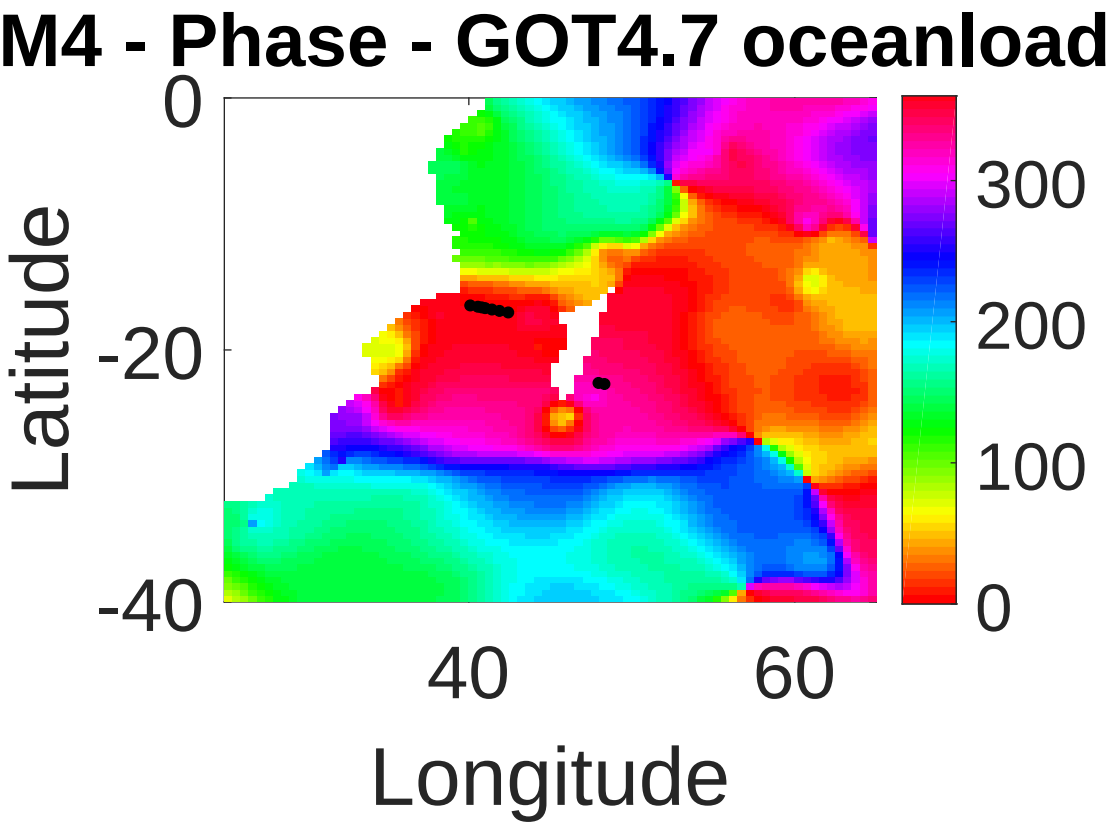

Figure 35: Phase for the M4 constituent. Black points indicate the locations of the measurement stations.

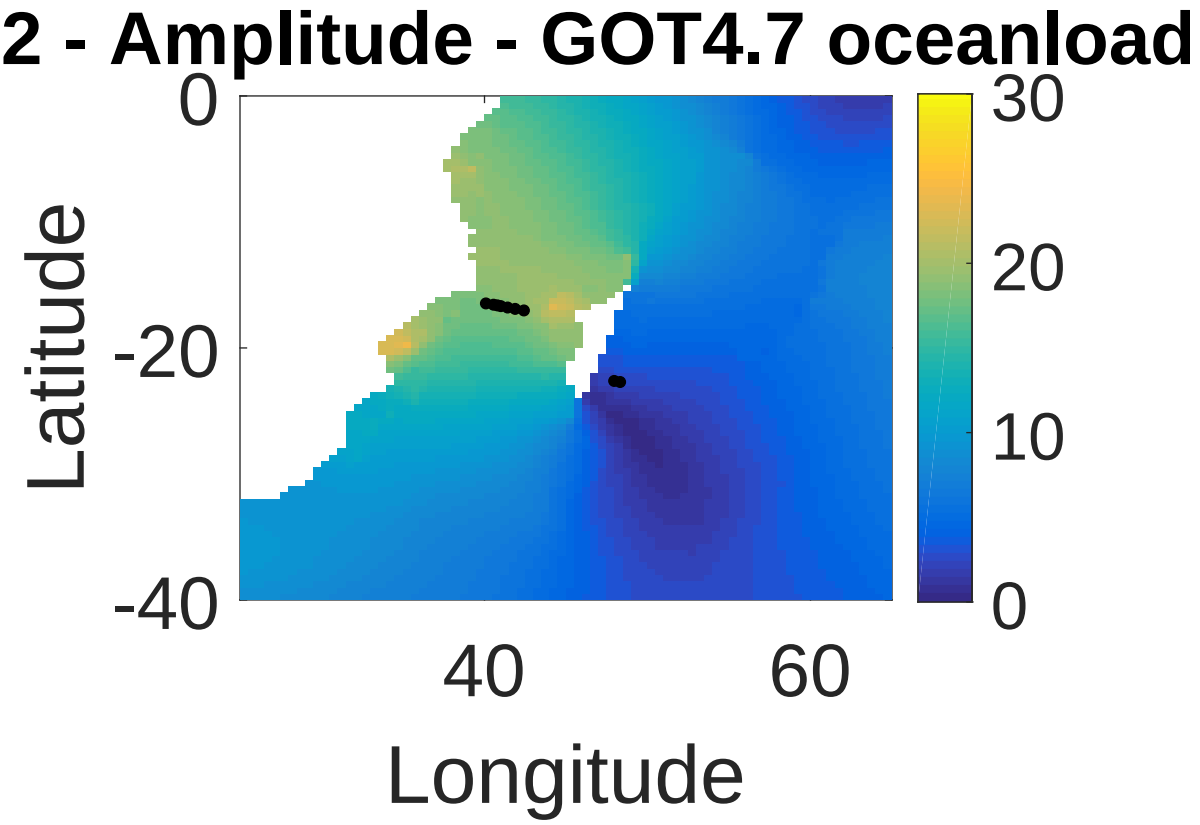

Figure 36: Amplitude for the N2 constituent. Black points indicate the locations of the measurement stations.

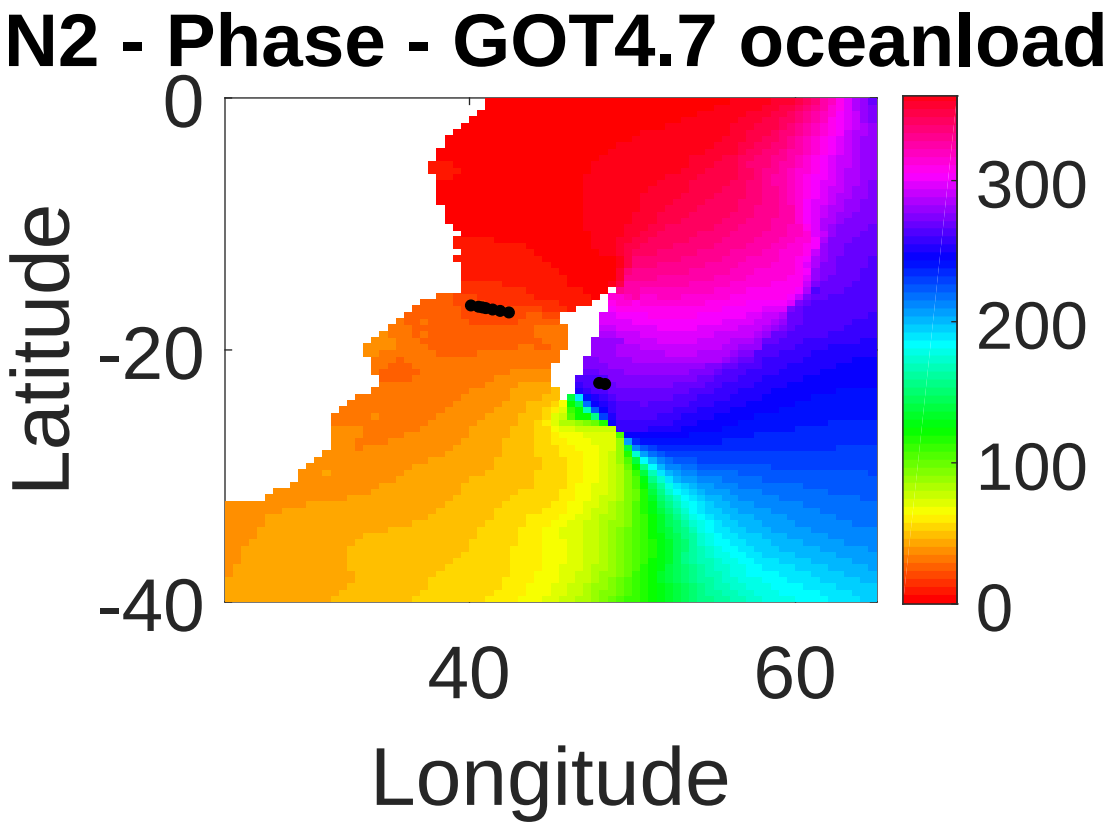

Figure 37: Phase for the N2 constituent. Black points indicate the locations of the measurement stations.

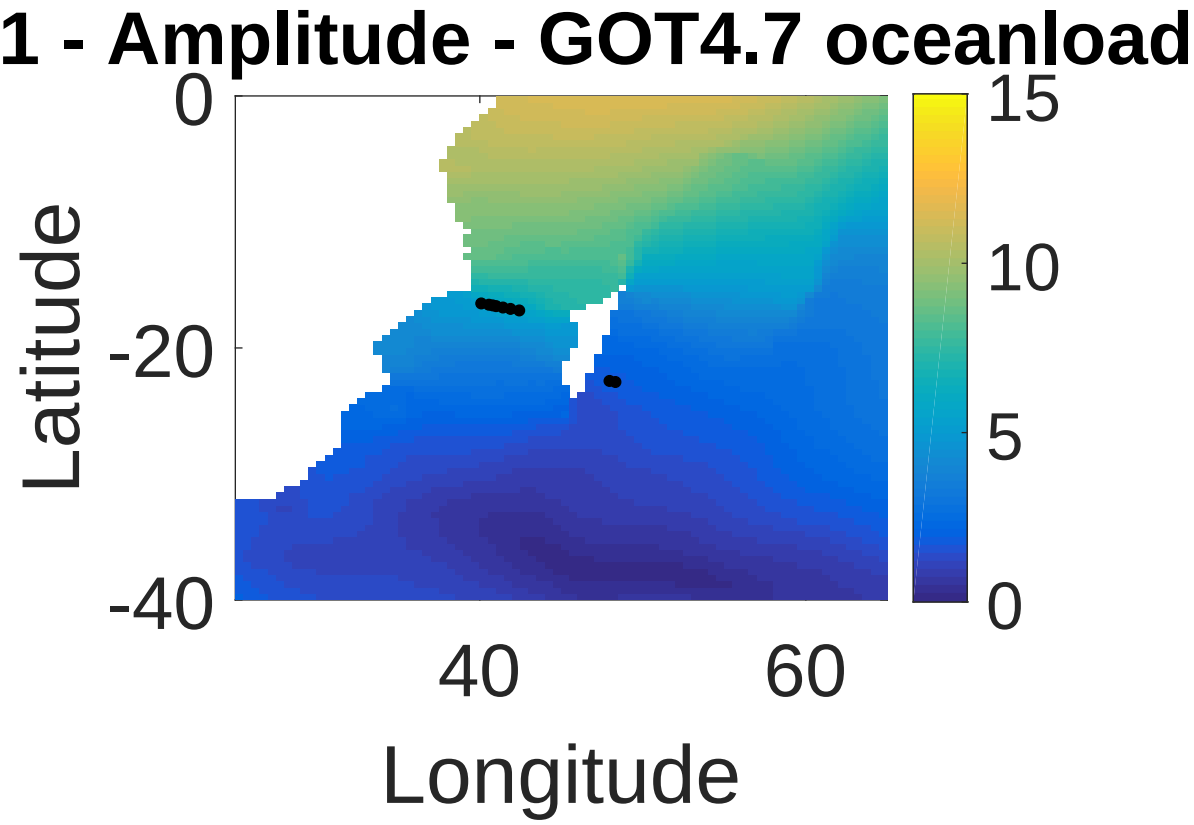

Figure 38: Amplitude for the O1 constituent. Black points indicate the locations of the measurement stations.

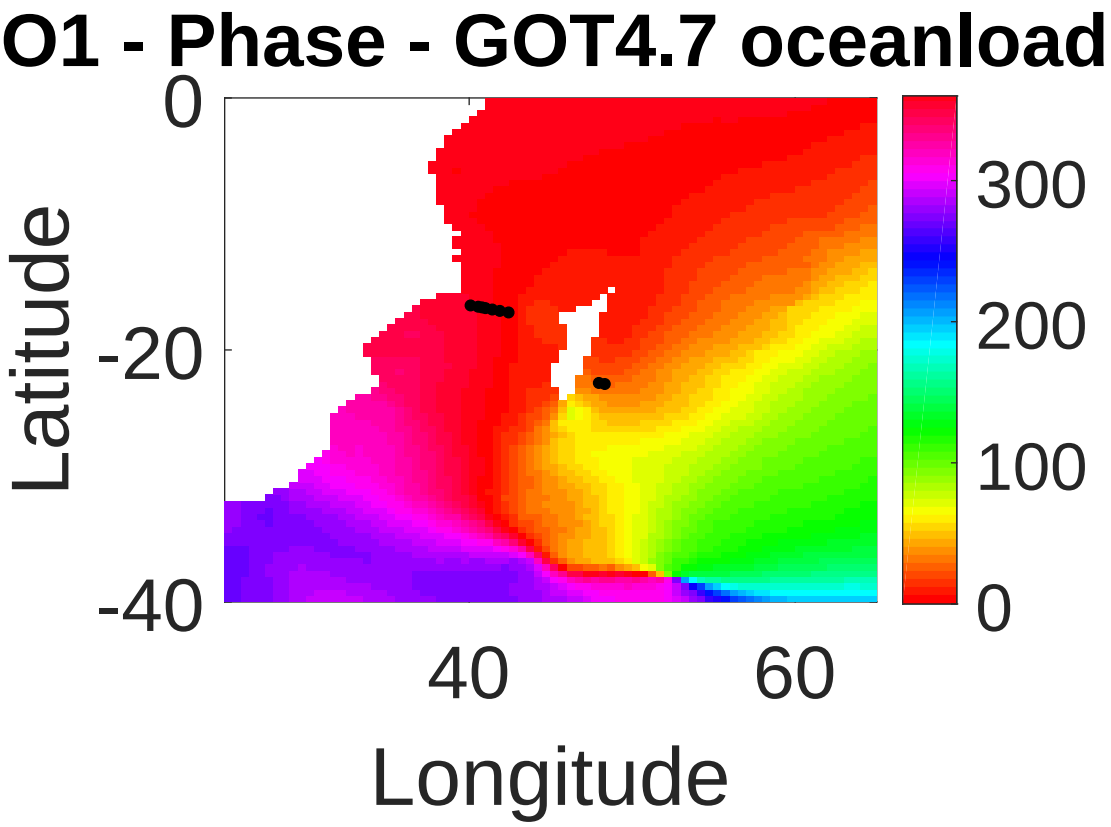

Figure 39: Phase for the O1 constituent. Black points indicate the locations of the measurement stations.

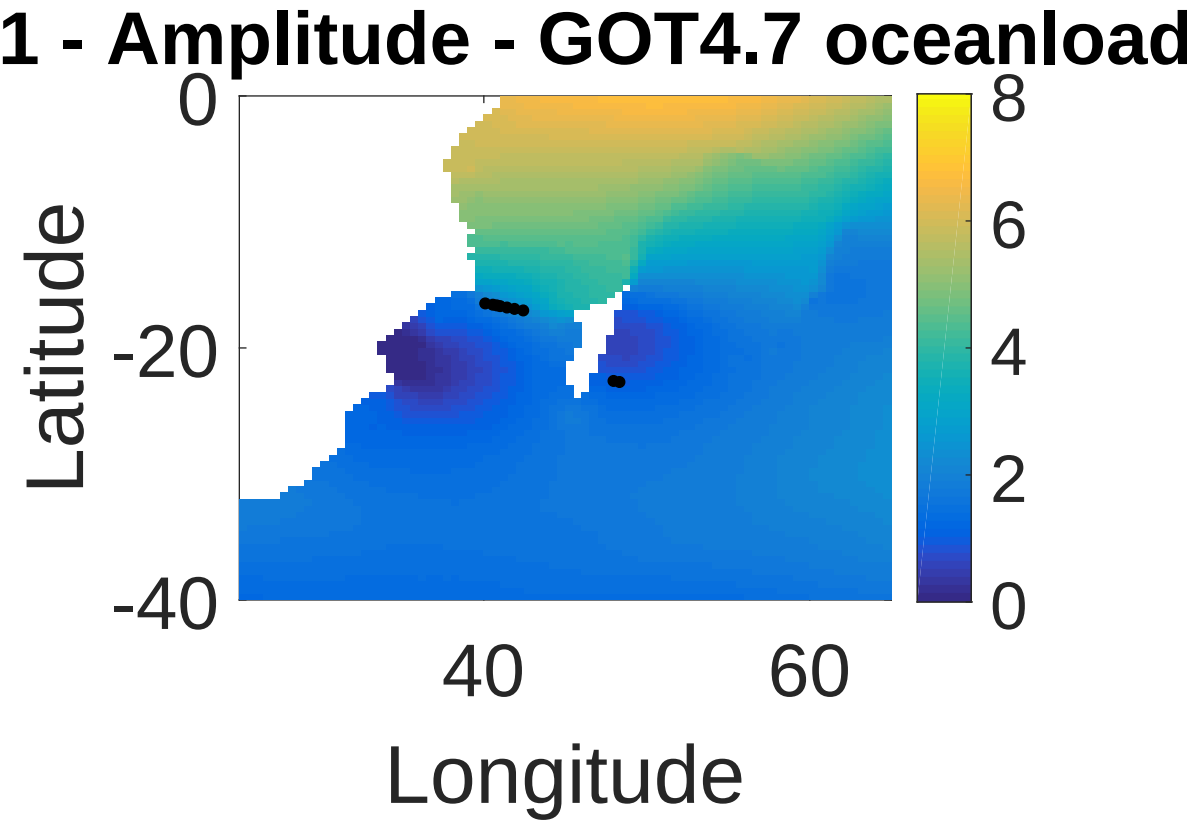

Figure 40: Amplitude for the P1 constituent. Black points indicate the locations of the measurement stations.

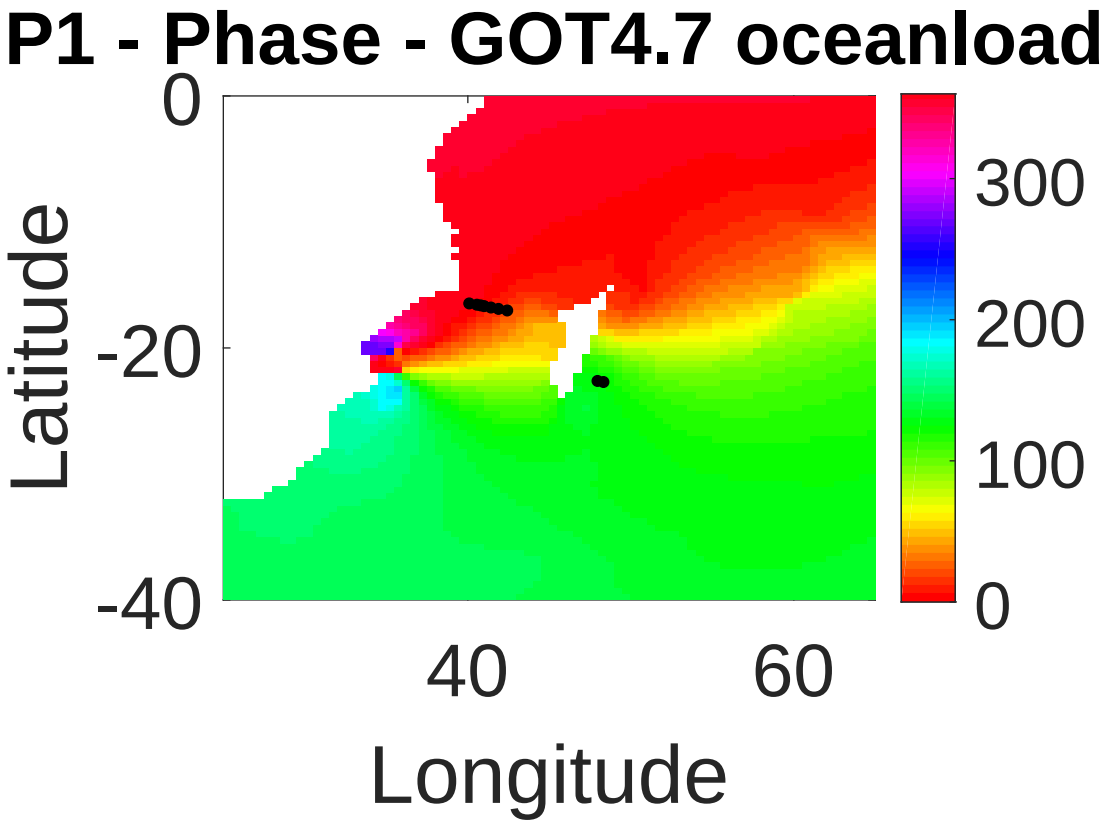

Figure 41: Phase for the P1 constituent. Black points indicate the locations of the measurement stations.

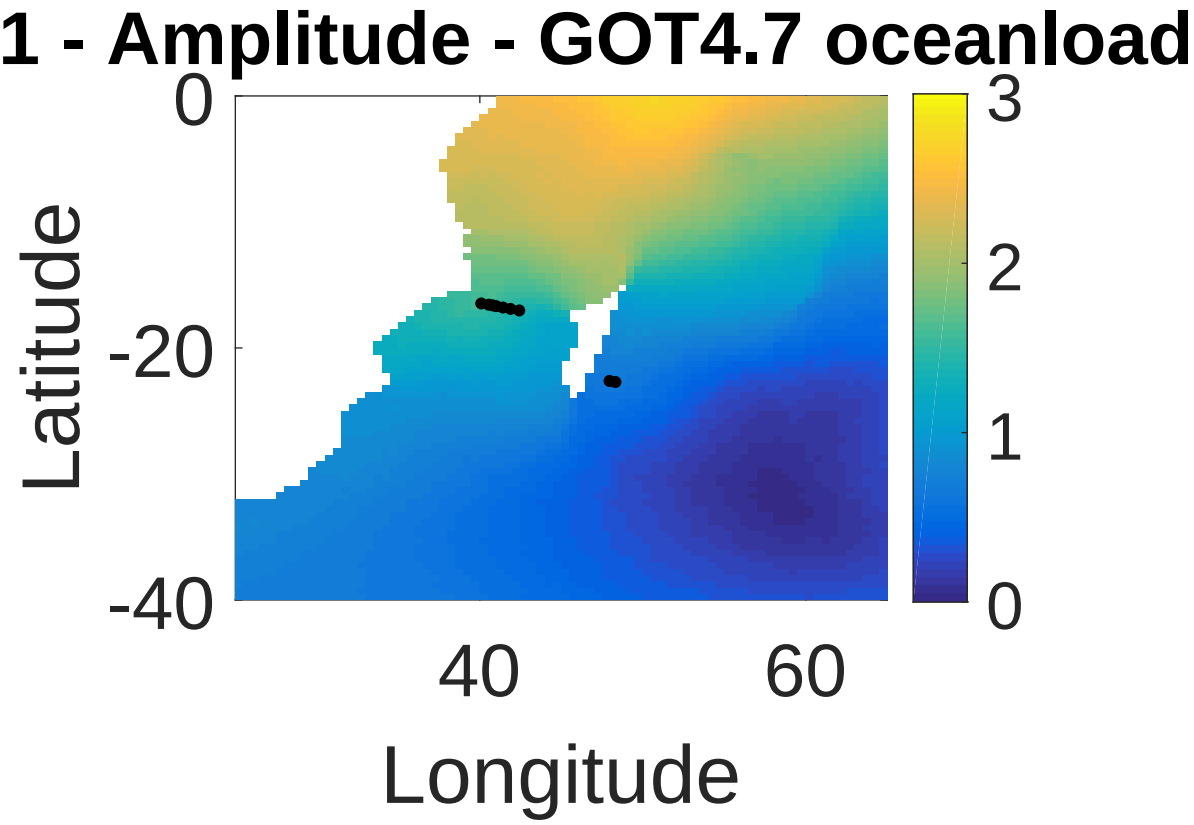

Figure 42: Amplitude for the Q1 constituent. Black points indicate the locations of the measurement stations.

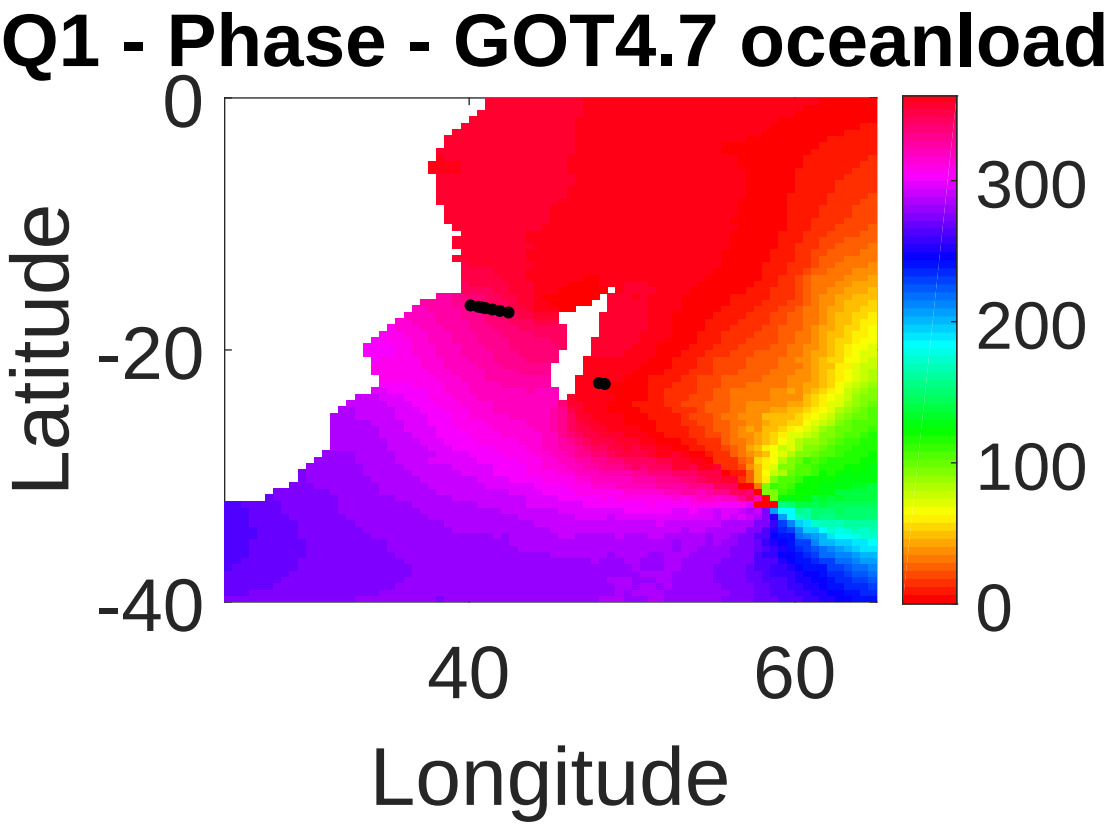

Figure 43: Phase for the Q1 constituent. Black points indicate the locations of the measurement stations.

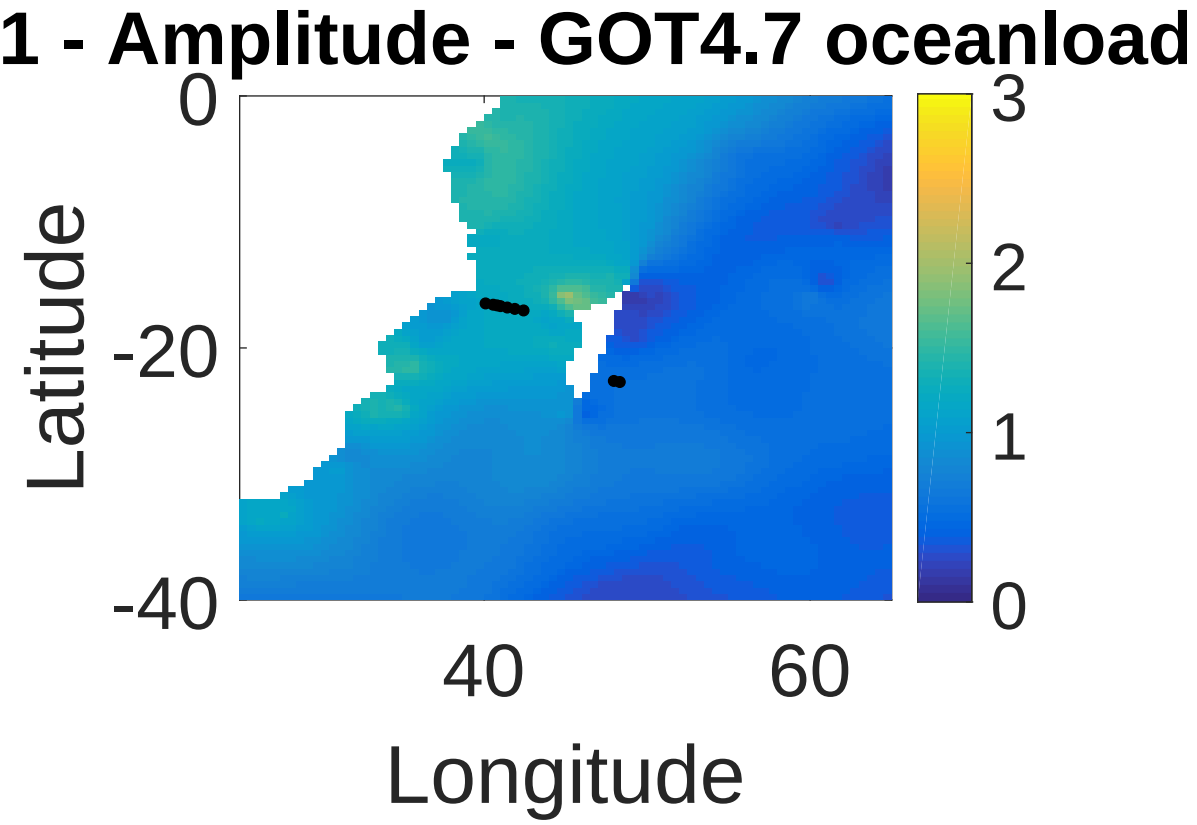

Figure 44: Amplitude for the S1 constituent. Black points indicate the locations of the measurement stations.

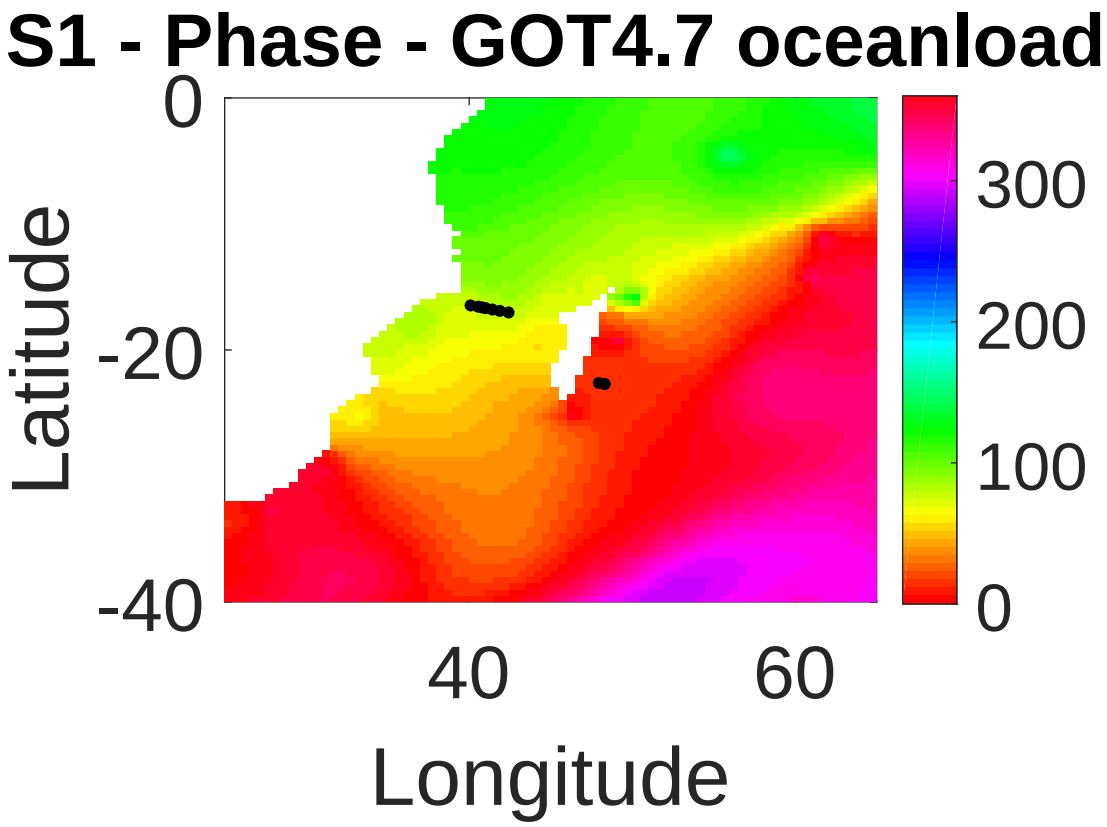

Figure 45: Phase for the S1 constituent. Black points indicate the locations of the measurement stations.

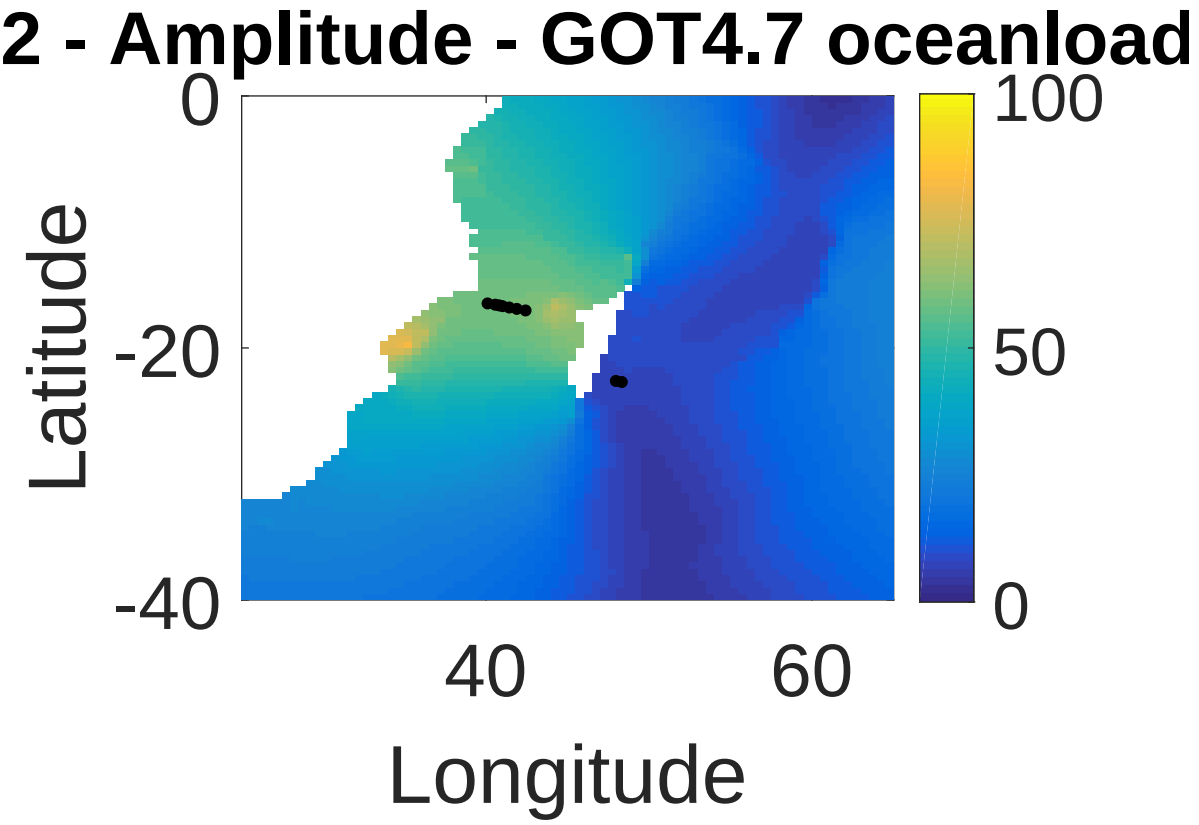

Figure 46: Amplitude for the S2 constituent. Black points indicate the locations of the measurement stations.

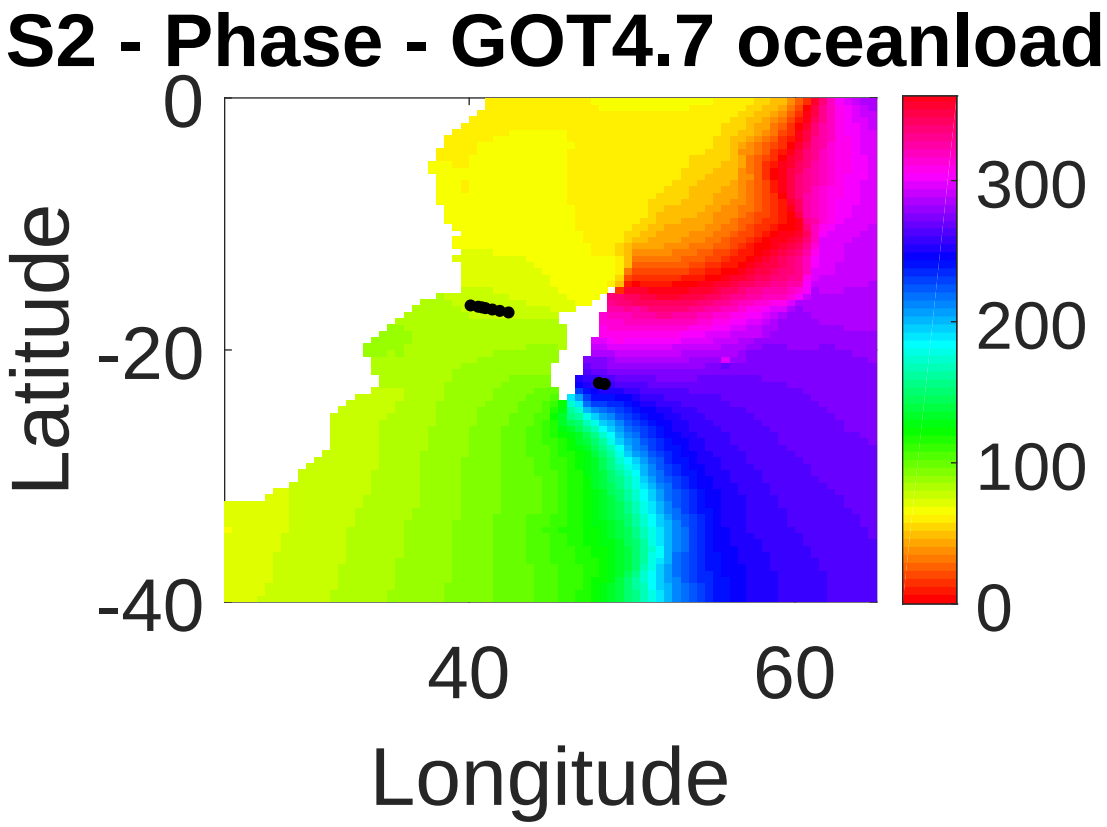

Figure 47: Phase for the S2 constituent. Black points indicate the locations of the measurement stations.

B.2 Altimeter data in tables

Amplitude

Tidal component	GOT4.7_oceantide		GOT4.7_oceanload		GOT4.10c_oceantide		GOT4.10c_oceanload	
	EMC1	EMC3	EMC1	EMC3	EMC1	EMC3	EMC1	EMC3
k1	3.0748	3.1196	3.0863	3.1173	3.286	3.361	3.0105	3.0516
k2	1.9677	1.9909	2.0568	2.0623	1.9805	1.9615	2.0597	2.023
m2	9.5549	9.35	10.1382	9.8117	9.7533	9.5967	10.1613	9.8983
m4	0.3638	0.3613	0.3538	0.3513	0.3638	0.3613	0.3538	0.3513
n2	2.4085	2.5518	2.4031	2.5167	2.5135	2.7485	2.4821	2.689
o1	1.8743	1.9062	1.7781	1.8085	2.2244	2.2383	1.898	1.9064
p1	0.9276	0.9415	0.9374	0.9472	0.9742	0.9968	0.8836	0.8959
q1	0.6923	0.692	0.6523	0.652	0.553	0.5663	0.4827	0.4886
s1	0.5743	0.5833	0.5543	0.5633	0.5743	0.5833	0.5543	0.5633
s2	6.8692	7.1279	7.1761	7.3703	6.7088	6.6921	7.0059	6.9289

Phase

Tidal component	GOT4.7_oceantide		GOT4.7_oceanload		GOT4.10c_oceantide		GOT4.10c_oceanload	
	EMC1	EMC3	EMC1	EMC3	EMC1	EMC3	EMC1	EMC3
k1	125.893	123.4543	126.6918	124.2319	114.8139	112.6949	122.5656	120.0816
k2	257.0561	256.9846	255.9211	255.8089	261.3556	261.0946	259.2691	258.9475
m2	261.3495	263.1786	256.0735	257.8404	260.2926	261.4184	255.508	256.6447
m4	327.7331	328.581	327.3699	328.2349	327.7331	328.581	327.3699	328.2349
n2	270.6759	273.4624	265.1316	268.3933	269.614	272.7288	264.9931	268.6836
o1	20.5947	21.1751	25.243	25.6786	29.0758	29.8961	29.9107	30.757
p1	121.9948	119.5063	122.9704	120.461	110.1959	108.1623	118.2056	115.7759
q1	353.8601	355.5928	352.1359	203.7228	351.5886	352.3877	350.89	351.7698
s1	14.0101	14.0485	12.9328	13.0526	14.0101	14.0485	12.9328	13.0526
s2	261.4144	261.6221	259.8914	260.1031	261.8502	262.1567	259.9082	260.1423

Figure 55: Altimeter data collected from the GOT-e model. This is the amplitude and phase data for both the EMC1 and EMC3 locations.

Amplitude

Constituent	GOT4_7_oceantide	GOT4_7_oceanload	GOT4_10c_oceantide	GOT4_10c_oceanload
k1	6.1751	5.8184	6.7009	6.1321
k2	16.952	16.38	17.089	16.516
m2	110.55	106.47	110.06	106.16
m4	0.75884	0.73884	0.75884	0.73884
n2	18.861	18.135	18.55	17.865
o1	5.9224	5.6331	6.1497	5.7104
p1	2.1002	1.9782	2.1891	2.0035
q1	1.6494	1.5694	1.6681	1.5652
s1	1.2266	1.183	1.2266	1.183
s2	60.7	58.627	60.967	58.914

(a) Altimeter data collected from the GOT-e model. This is the amplitude data at the lmc4 location.

Phase

Constituent	GOT4_7_oceantide	GOT4_7_oceanload	GOT4_10c_oceantide	GOT4_10c_oceanload
k1	228.13	228.79	2.2094	229.33
k2	75.401	75.518	75.016	75.207
m2	36.338	36.349	36.592	36.654
m4	1.6118	25.37	1.6118	25.37
n2	18.002	18.005	17.444	17.491
o1	353.67	354.51	355.84	354.73
p1	251.51	228.34	1.5799	228.84
q1	332.44	332.81	336.08	335.07
s1	76.924	76.483	76.924	76.483
s2	76.303	76.414	76.868	77.03

(b) Altimeter data collected from the GOT-e model. This is the phase data at the lmc4 location.

Amplitude

Constituent	GOT4_7_oceantide	GOT4_7_oceanload	GOT4_10c_oceantide	GOT4_10c_oceanload
k1	6.4663	6.0928	6.9958	6.3797
k2	17.043	16.423	17.149	16.528
m2	111.65	107.24	111.04	106.81
m4	0.71543	0.69543	0.71543	0.69543
n2	19.099	18.317	18.753	18.013
o1	5.9907	5.6814	6.2121	5.7505
p1	2.1903	2.0632	2.2739	2.0746
q1	1.6161	1.5361	1.6618	1.5518
s1	1.2423	1.1923	1.2423	1.1923
s2	61.127	58.874	61.288	59.055

(a) Altimeter data collected from the GOT-e model. This is the amplitude data at the lmc5 location.

Phase

Constituent	GOT4_7_oceantide	GOT4_7_oceanload	GOT4_10c_oceantide	GOT4_10c_oceanload
k1	2.5829	3.3847	5.9316	3.6748
k2	74.974	75.084	74.545	74.735
m2	36.117	36.131	36.41	36.477
m4	2.2795	2.2063	2.2795	2.2063
n2	17.487	17.493	16.817	16.855
o1	355.56	356.45	358.06	357.08
p1	1.9108	2.7174	5.1739	3.0302
q1	334.56	335	338.5	337.59
s1	77.973	77.583	77.973	77.583
s2	76.16	76.273	76.623	76.789

(b) Altimeter data collected from the GOT-e model. This is the phase data at the lmc5 location.

Amplitude

Constituent	GOT4_7_oceantide	GOT4_7_oceanload	GOT4_10c_oceantide	GOT4_10c_oceanload
k1	6.715	6.3381	7.2408	6.5922
k2	17.137	16.495	17.224	16.582
m2	112.57	108.03	111.86	107.49
m4	0.67544	0.65544	0.67544	0.65544
n2	19.309	18.5	18.941	18.173
o1	6.0319	5.7158	6.2504	5.7737
p1	2.2672	2.1412	2.3457	2.1397
q1	1.572	1.4908	1.6389	1.5283
s1	1.2525	1.2025	1.2525	1.2025
s2	61.521	59.198	61.583	59.278

(a) Altimeter data collected from the GOT-e model. This is the amplitude data at the lmc5a location.

Phase

Constituent	GOT4_7_oceantide	GOT4_7_oceanload	GOT4_10c_oceantide	GOT4_10c_oceanload
k1	6.4654	7.3891	9.4152	7.4865
k2	74.726	74.832	74.246	74.431
m2	36.039	36.061	36.372	36.447
m4	2.6024	2.5417	2.6024	2.5417
n2	17.245	17.257	16.527	16.569
o1	357.36	313.16	314.99	314.13
p1	5.6237	6.5422	8.5457	6.7045
q1	336.32	336.84	340.42	339.59
s1	78.585	78.23	78.585	78.23
s2	76.095	76.212	76.486	76.652

(b) Altimeter data collected from the GOT-e model. This is the phase data at the lmc5a location.

Amplitude

Constituent	GOT4_7_oceantide	GOT4_7_oceanload	GOT4_10c_oceantide	GOT4_10c_oceanload
k1	6.9195	6.5326	7.4209	6.7496
k2	17.226	16.569	17.294	16.637
m2	113.36	108.71	112.56	108.08
m4	0.65149	0.63149	0.65149	0.63149
n2	19.483	18.654	19.101	18.315
o1	6.0435	5.7213	6.2562	5.767
p1	2.3285	2.1964	2.3967	2.1845
q1	1.5462	1.4566	1.6231	1.5106
s1	1.2691	1.2191	1.2691	1.2191
s2	61.918	59.538	61.89	59.521

(a) Altimeter data collected from the GOT-e model. This is the amplitude data at the lmc6 location.

Phase

Constituent	GOT4_7_oceantide	GOT4_7_oceanload	GOT4_10c_oceantide	GOT4_10c_oceanload
k1	9.8901	10.923	12.569	10.922
k2	74.643	74.757	74.127	74.314
m2	36.082	36.116	36.436	36.521
m4	2.4893	2.4222	2.4893	2.4222
n2	17.238	17.262	16.53	16.585
o1	358.99	15.322	17.484	16.738
p1	8.9085	9.9336	11.615	10.038
q1	338.23	338.82	342.27	341.53
s1	78.73	78.403	78.73	78.403
s2	76.091	76.218	76.432	76.606

(b) Altimeter data collected from the GOT-e model. This is the phase data at the lmc6 location.

Amplitude

Constituent	GOT4_7_oceantide	GOT4_7_oceanload	GOT4_10c_oceantide	GOT4_10c_oceanload
k1	7.1968	6.8151	7.6963	7.0079
k2	17.342	16.683	17.404	16.744
m2	114.32	109.65	113.46	108.97
m4	0.6311	0.6111	0.6311	0.6111
n2	19.695	18.865	19.333	18.543
o1	6.0809	5.7605	6.2832	5.7924
p1	2.4132	2.2828	2.4824	2.2632
q1	1.5057	1.4157	1.5868	1.4764
s1	1.2792	1.2292	1.2792	1.2292
s2	62.418	60.037	62.335	59.965

(a) Altimeter data collected from the GOT-e model. This is the amplitude data at the lmc7 location.

Phase

Constituent	GOT4_7_oceantide	GOT4_7_oceanload	GOT4_10c_oceantide	GOT4_10c_oceanload
k1	13.729	14.854	16.095	14.771
k2	74.647	74.766	74.128	74.326
m2	36.159	36.198	36.5	36.598
m4	1.8966	1.827	1.8966	1.827
n2	17.4	17.438	16.724	16.8
o1	44.034	2.1108	4.5212	3.9222
p1	12.621	13.746	15.069	13.798
q1	340.44	341.14	343.9	343.22
s1	78.535	78.224	78.535	78.224
s2	76.04	76.17	76.353	76.532

(b) Altimeter data collected from the GOT-e model. This is the phase data at the lmc7 location.

Amplitude

Constituent	GOT4_7_oceantide	GOT4_7_oceanload	GOT4_10c_oceantide	GOT4_10c_oceanload
k1	7.5353	7.156	8.0437	7.3311
k2	17.512	16.854	17.551	16.902
m2	115.45	110.79	114.62	110.15
m4	0.61984	0.59984	0.61984	0.59984
n2	19.973	19.145	19.643	18.857
o1	6.1119	5.7959	6.3023	5.8068
p1	2.513	2.3872	2.5796	2.3521
q1	1.4532	1.3729	1.5709	1.4534
s1	1.2759	1.2259	1.2759	1.2259
s2	63.133	60.761	63.038	60.676

(a) Altimeter data collected from the GOT-e model. This is the amplitude data at the lmc8 location.

Phase

Constituent	GOT4_7_oceantide	GOT4_7_oceanload	GOT4_10c_oceantide	GOT4_10c_oceanload
k1	18.734	19.993	20.6	19.678
k2	75.038	75.174	74.531	74.746
m2	36.564	36.629	36.853	36.969
m4	75.068	74.966	75.068	74.966
n2	18.03	18.107	17.493	17.603
o1	4.0991	5.2623	7.6103	7.2057
p1	17.512	18.761	19.49	18.595
q1	342.64	343.45	346.08	345.51
s1	77.636	77.317	77.636	77.317
s2	76.157	76.3	76.473	76.659

(b) Altimeter data collected from the GOT-e model. This is the phase data at the lmc8 location.

Amplitude

Constituent	GOT4_7_oceantide	GOT4_7_oceanload	GOT4_10c_oceantide	GOT4_10c_oceanload
k1	6.6098	6.2349	7.1389	6.5048
k2	17.093	16.46	17.188	16.556
m2	112.15	107.67	111.49	107.19
m4	0.69182	0.67182	0.69182	0.67182
n2	19.216	18.42	18.857	18.102
o1	6.0188	5.7058	6.2386	5.7686
p1	2.2348	2.1088	2.3158	2.1128
q1	1.5918	1.5118	1.6496	1.5396
s1	1.247	1.197	1.247	1.197
s2	61.331	59.04	61.438	59.168

(a) Altimeter data collected from the GOT-e model. This is the amplitude data at the lmctrap location.

Phase

Constituent	GOT4_7_oceantide	GOT4_7_oceanload	GOT4_10c_oceantide	GOT4_10c_oceanload
k1	4.6088	5.4736	7.7419	5.6608
k2	74.811	74.918	74.359	74.546
m2	36.047	36.063	36.361	36.433
m4	2.5243	2.4596	2.5243	2.4596
n2	17.322	17.33	16.617	16.656
o1	356.52	357.43	359.16	358.24
p1	3.8498	4.7136	6.9279	4.9457
q1	335.5	335.97	339.53	338.66
s1	78.378	78.007	78.378	78.007
s2	76.106	76.22	76.527	76.692

(b) Altimeter data collected from the GOT-e model. This is the phase data at the lmctrap location.